# Atmospheric new particle formation characteristics in the Arctic as measured at Mount Zeppelin, Svalbard, from 2016 to 2018

Haebum Lee[1], KwangYul Lee[1], Chris Rene Lunder[2], Radovan Krejci[3], Wenche Aas[2], Jiyeon Park[4], Ki-Tae Park[4], Bang Yong Lee[4], Young-Jun Yoon[4,*], and Kihong Park[1,*]

[1]School of Earth Sciences and Environmental Engineering, Gwangju Institute of Science and Technology, 123 Cheomdangwagiro, Buk-gu, Gwangju 61005, Republic of Korea.
[2]Department for Atmospheric and Climate Research, NILU - Norwegian Institute for Air Research, Kjeller, Norway.
[3]Department of Environmental Sciences and the Bolin Centre for Climate Research, Stockholm University, Stockholm, SE-106 91, Sweden.
[4]Korea Polar Research Institute, 26, Songdo Mirae-ro, Yeonsu-Gu, Incheon, Korea.

*Correspondence to: Kihong Park (kpark@gist.ac.kr) and Young-Jun Yoon (yjyoon@kopri.re.kr)

**Abstract.** We conducted continuous measurement of nanoparticles down to 3 nm size in the Arctic at Mount Zeppelin, Ny Ålesund, Svalbard, from 2016 to 2018, providing a size distribution of nanoparticles (3–60 nm) with a higher size resolution than ever before. A significant number of nanoparticles as small as 3 nm were often observed during new particle formation (NPF), particularly in summer, suggesting that these were likely produced near the site rather than being transported from other regions after growth. The average NPF frequency per year was 23% having the highest percentage in August (63%). The average formation rate (J) and growth rate (GR) for 3–7 nm particles were 0.04 cm$^{-3}$ s$^{-1}$ and 2.07 nm h$^{-1}$, respectively. Although NPF frequency in the Arctic was comparable to that in continental areas, the J and GR were much lower. The number of nanoparticles increased more frequently when air mass originated over the south and southwest ocean regions; this pattern overlapped with regions having strong chlorophyll-α concentration and dimethyl sulfide (DMS) production capacity (southwest ocean), and was also associated with increased $NH_3$ and $H_2SO_4$ concentration, suggesting that marine biogenic sources were responsible for gaseous precursors to NPF. Our results show that previously developed NPF occurrence criteria (low loss rate and high cluster growth rate favor NPF) are also applicable to NPF in the Arctic.

## 1 Introduction

The Arctic climate system is affected by the region's snow-covered land, sea ice, and ocean, making the region vulnerable to global climate change (Jeffries and Richter-Menge, 2012). Greenhouse gases and aerosols are significant factors affecting the regional climate (Quinn et al., 2007; IPCC, 2014). In particular, aerosols in the ambient atmosphere affect the radiation balance by scattering or absorbing incoming solar light (direct effect) (Toon and Pollack, 1980; Satheesh et al., 2005) and forming clouds by acting as cloud condensation nuclei (CCN) (indirect effect) (Merikanto et al., 2009).

New particle formation (NPF), which significantly enhances the number of particles in the ambient atmosphere, has been observed in various locations and at various times (Kulmala et al., 2004; Wang et al., 2017; Yu et al., 2017). In favourable conditions, newly formed nanoparticles can, through condensation and coagulation, grow to sizes allowing the formation of CCN. NPF is observed regardless of pollution level, from very clean (e.g., background sites) to heavily polluted (e.g., urban sites), suggesting that various pathways are involved depending on the location and time (Kulmala et al., 2004; Wang et al., 2017). Nucleation can occur almost anywhere in diverse environments, but NPF is observed only when freshly nucleated clusters grow to a detectable size (1–3 nm) (McMurry et al., 2010). Previously developed criteria for NPF occurrence suggest that a low loss (or scavenging) rate and high growth rate (GR) of clusters increase fresh nuclei survival probability and thus favoring NPF, while a high loss rate and low cluster GR suppress it (Kuang et al., 2012).

In the Arctic, specific phenomenon called "Arctic haze" related to long range transport of polluted air masses typically occurs in the late winter and early spring (Iziomon et al., 2006; O'Neill et al., 2008, Hirdman et al., 2010). The Arctic haze is associated with elevated concentrations of accumulation-mode particles. (Radke et al., 1984; Shaw, 1995; Law and Stohl, 2007; Quinn et al., 2007). High concentration of accumulation-mode particles results in a high condensational sink (CS) for precursor vapors, which could suppress NPF. The NPF in the Arctic was often reported in summer, when the CS was smaller (Wiedensohler et al., 1996; Covert et al., 1996; Sharma et al., 2013; Willis et al., 2016; Croft et al., 2016). In addition, strong biogenic production from marine and coastal environments in the Arctic region (e.g., Alaska, Alert, and Svalbard) was reported to be linked to NPF due to an increased amount of biogenic sulfur compounds such as dimethyl sulfide and its oxidative products (methane sulfonate and biogenic sulfate) (Leaitch et al., 2013; Park et al., 2017). Like in sulfuric acid-rich regions, organic-based new particles were observed in pristine environments (Quinn et al., 2002; Karl et al., 2013; Leaitch et al., 2013; Heintzenberg et al., 2015). Asmi et al. (2016) reported that NPF was more common in air masses of oceanic origin compared to continental ones in the Arctic (Tiksi station, Russia). Dall'Osto et al. (2018) suggested that NPF at Station Nord in North Greenland was related to seasonal sea-ice cycles (i.e., the NPF was associated with air masses coming from open water and melting sea-ice regions).

There are several past studies of NPF at the Zeppelin Observatory at Mount Zeppelin in Svalbard, Norway (Tunved et al., 2013; Dall'Osto et al., 2017; Heintzenberg et al., 2017). The location of the station is 474 m above sea level and ~2 km from a small scientific community, with minimal effects from anthropogenic sources; its unique geographical location is ideal for investigating NPF in the Arctic environment. Tunved et al. (2013) studied seasonal variations in particle size distribution and NPF based on aerosol size distribution data (10–790 nm) from 2000 to 2010. Heintzenberg et al. (2017) developed a new NPF search algorithm using size distribution data (5–630 nm) from 2006 to 2015. Dall'Osto et al. (2017) determined the relationship between NPF and the extent of Arctic sea-ice melt using size distribution data (10–500 nm) from 2000 to 2010 and used hourly data to classify the size distributions and NPF types. It was reported that NPF at the Mount Zeppelin site mostly occur during summer, which was attributed to the low CS and high biological activity in summer (Leaitch et al., 2013; Heintzenberg et al., 2015; Park et al., 2017). NPF occurrence was low during the Arctic haze (with high CS) period (Tunved et al., 2013; Croft et al., 2016). Heintzenberg et al. (2017) suggested that NPF at the Mount Zeppelin site was related to solar

65 flux and sea surface temperature, affecting marine biological processes and photochemical reactions with less CS. They
66 reported the potential source regions for NPF to be the marginal-ice and open-water areas between northeastern Greenland and
67 eastern Svalbard. Although particle size distribution data from the Mount Zeppelin site are available (Ström et al., 2003;
68 Tunved et al., 2013; Dall'Osto et al., 2017; Heintzenberg et al., 2017), no data regarding the size distribution of nanoparticles
69 smaller than 5 nm are available, though these could provide greater insight into NPF characteristics. Currently, the initial
70 formation and growth of nanoparticles below 10 nm cannot be resolved, and weak NPF events with no substantial particle
71 growth up to 10 nm cannot be detected.

72 In this study, we measured number size distribution of nanoparticles down to 3 nm for the first time at Zeppelin
73 station, and obtained continuous size distributions of 3–60 nm particles every 3 min from 2016 to 2018. This allowed the size
74 distribution of nanoparticles to be determined with a higher size resolution than ever before, enabling better identification of
75 whether freshly nucleated particles formed on-site or were transported from other regions after substantial growth. We were
76 also able to detect NPF events when particle growth was terminated below 10 nm. The particle size distributions were classified
77 into several clusters, and the seasonal (monthly), daily, and diurnal variations of the nanoparticle concentrations were examined.
78 We also applied the NPF criteria to Arctic data to determine whether or not NPF should occur and investigated the
79 characteristics of NPF events related to formation rate, GR, CS, and meteorological parameters. Finally, potential source
80 regions for NPF were explored using air mass backward trajectory and satellite-derived chlorophyll-α concentration data. The
81 chlorophyll-α which is involved in oxygenic photosynthesis in ocean has been considered as a proxy for phytoplankton biomass
82 only. Recent studies showed that there was a strong correlation between sea-surface chlorophyll-α concentration (estimated
83 by MODIS-aqua) and atmospheric DMS levels at Zeppelin station (Park et al., 2013; Park et al., 2018).

84 **2 Methods**

85 The measurement site was located at the Zeppelin Observatory at Mount Zeppelin, Svalbard (78º54'N, 11º53'E),
86 which is 474 m above sea level and ~2 km from the small scientific community in Ny-Ålesund, Norway (78º55'N, 11º56'E)
87 (Figure 1). Ny-Ålesund lies within the west Spitsbergen current at the northernmost point of the warm Atlantic influx; this
88 location provides an ideal location for observing climate parameters and investigating the long-range transport route by which
89 contamination is often carried via southerly air masses (Neuber et al., 2011). The dominant wind patterns (east and southeast
90 from the Kongsvegen glacier (40%) and northwest from the Kongsfjorden channels (14%) during the measurement period)
91 and elevation suggest that the effects of local sources on the Zeppelin Observatory are small (Beine et al., 2001).

92 An air inlet with a flow rate of 100 L min$^{-1}$ was used to introduce ambient aerosols into the instruments. The flow
93 temperature was maintained above 0°C to prevent ice and frost formation in the tube. The observatory was kept warm and dry,
94 with an indoor temperature and relative humidity (RH) of ~20°C and < 30%, respectively (Tunved et al., 2013; Heintzenberg
95 et al., 2017). A nano-scanning mobility particle sizer consisting of a nano-differential mobility analyzer (nano-DMA) (model
96 3085, TSI, USA) and an ultrafine condensation particle counter (model 3776, TSI, USA) was used to measure the size

97 distribution of nanoparticles (3–60 nm) every 3 min; the aerosol flow rate was 1.5 L min$^{-1}$ and the sheath flow rate was 15 L

98 min$^{-1}$. The size distribution data were processed using the method described by Kulmala et al. (2012).

99 Daily ionic species (Na$^+$, Mg$^{2+}$, K$^+$, NH$_4^+$, NO$_3^-$, SO$_4^{2-}$, and Cl$^-$) in particulate matters and gas data (NH$_3$ and SO$_2$)

100 at Zeppelin Observatory, along with meteorological parameters (temperature, RH, wind, and pressure), were obtained from

101 the Norwegian national monitoring program (Aas et al., 2019) via the EBAS database (http://ebas.nilu.no/). Daily ionic species

102 and gas data are daily measurements collected with a 3-stage filterpack sampler (NILU prototype) with no pre-impactor. The

103 size cut off of the inlet section is approximately 10 µm. Field blanks were prepared in the same as the other samples. It should

104 be noted that for the nitrogen compounds the separation of gas and aerosol might be biased due to the volatile nature of NH$_4$NO$_3$.

105 The detection limits were 0.05 µg N m$^{-3}$ and 0.01 µg S m$^{-3}$ for NH$_3$ and SO$_2$, respectively, and 0.01 µg m$^{-3}$ for Na$^+$, Mg$^{2+}$, K$^+$,

106 NH$_4^+$, and Cl$^-$, 0.01 µg N m$^{-3}$ for NO$_3^-$, and 0.01 µg S m$^{-3}$ for SO$_4^{2-}$. The data quality management and system are accredited

107 in accordance to NS-EN ISO / IEC 1702 standards. The detailed information of sampling method and analysis can be found

108 elsewhere (EMAP 2014; Aas et al., 2019). Solar radiation (SRAD) at the AWIPEV (the Alfred Wegener Institute Helmholtz

109 Centre for Polar and Marine Research and the French Polar Institute Paul Emile Victor) observatory in Ny-Ålesund were

110 obtained from the Baseline Surface Radiation Network (BSRN) (Maturilli, 2019). Hourly data for number size distributions

111 of particles from 5–810 nm and 10–790 nm, measured with discrete mobility particle sizers (DMPS), were obtained from

112 Stockholm University and the Norwegian Institute for Air Research (NILU), respectively. The data from the DMPS and

113 filterpack measurements are reported to several international monitoring programmes (EMEP (European Monitoring and

114 Evaluation Programme), ACTRIS (Aerosols, Clouds and Trace gases Research InfraStructure Network), and GAW-WDCA

115 (Global Atmospheric Watch-the World Data Centre for Aerosols)), and they are openly available from the database

116 infrastructure EBAS. In addition, the hourly black carbon (BC) data at Zeppelin were used to examine the effect of primary

117 combustion sources on the NPF.

118 Satellite-derived chlorophyll-α concentration data in the Svalbard region (70–85ºN, 25ºW–50ºE) was obtained from

119 the level-3 product of the Aqua-Moderate Resolution Imaging Spectroradiometer (MODIS) at a 4 km resolution. Air mass

120 backward trajectories arriving at the Zeppelin Observatory were calculated for up to 5 days using the National Oceanic and

121 Atmospheric Administration (NOAA) Hybrid Single Particle Lagrangian Integrated Trajectory (HYSPLIT) model based on

122 Global Data Assimilation System (GDAS) 1° data. A potential source contribution function (PSCF) method (Pekney et al.,

123 2006; Wang et al., 2009; Fleming et al., 2012) was also used to relate the air mass to NPF occurrence by analyzing the residence

124 time of the air mass relative to the concentration of nanoparticles at the receptor site (Wang et al., 2009). In addition, the k-

125 means clustering method, an unsupervised data classification/partitioning approach, was used to classify potential air mass

126 origin along with the size distributions (Beddows et al., 2009; Dall'Osto et al., 2017).

127 The particle GR was calculated as the change rates of representative particle diameters (d$_1$ and d$_2$) with the highest

128 concentrations at particular times (t$_1$ and t$_2$) (Hussein et al., 2005; Kulmala et al., 2012). The CS, which determines how rapidly

129 condensable vapor molecules will condense on the existing aerosols (Kulmala et al., 2012), was calculated from the size

130 distribution data (3–810 nm) with an assumed H$_2$SO$_4$ diffusion coefficient of 0.117 cm$^{-2}$ s$^{-1}$ (Gong et al., 2010; Cai et al., 2017).

131    The number concentration in the size range $d_i$ to $d_j$ ($N_{i-j}$) was derived from the measured size distribution data. Considering the

132    particle loss and production processes allowed the following balance equation for $N_{i-j}$ to be derived:

133

$$\frac{dN_{i-j}}{dt} = J_{i-j} - F_{coag} - F_{growth} \quad (1)$$

134

135

136    where $J_{i-j}$ is the particle formation rate in the size range of $d_i$ to $d_j$, $F_{coag}$ is the particle loss rate related to coagulation scavenging

137    in the size range of $d_i$ to $d_j$, and $F_{growth}$ is the condensational GR of the nucleation-mode particles. Based on methods suggested

138    by Kulmala et al. (2012), the particle formation rate ($J_{i-j}$) was calculated as:

139

$$J_{i-j} = \frac{dN_{i-j}}{dt} + \frac{N_{i-j}}{d_j - d_i} \cdot GR + N_{i-j}CoagS_{i-j} \quad (2)$$

140

141

142    where $CoagS_{i-j}$ represents the mean of the coagulation sink (CoagS) in the size range of $d_i$ to $d_j$.

143          The dimensionless criterion ($L_\Gamma$), which can be used to predict the occurrence of NPF events (McMurry et al., 2005;

144    Cai et al., 2017), was calculated as:

145

$$L_\Gamma = \frac{\bar{c}_1 A_{Fuchs}}{4\beta_{11}N_1\Gamma} \quad (3)$$

146

147

148    where $\bar{c}_1$ is the mean thermal velocity of vapor ($H_2SO_4$), $A_{Fuchs}$ is the Fuchs surface area (a coagulation scavenging parameter),

149    $\beta_{11}$ is the free molecule collision frequency function for monomer collisions, $N_1$ is the $H_2SO_4$ molecular concentration during

150    the nucleation event, and $\Gamma$ is the growth enhancement factor obtained by dividing the measured GR by the growth determined

151    based on the condensation of only $H_2SO_4$. The $H_2SO_4$ molecular concentration was predicted from the measured daily $SO_2$,

152    hourly CS, hourly solar radiation, and hourly meteorological data (RH and temperature) using the method proposed by

153    Mikkonen et al. (2011). The empirical proxy model of $H_2SO_4$ is given by:

154

$$[H_2SO_4] = a \cdot k \cdot [SO_2]^b \cdot SRAD^c \cdot (CS \cdot RH)^d \quad (4)$$

155

156

157    where $[SO_2]$ is the $SO_2$ molecular concentration (molecules cm$^{-3}$), SRAD is the solar radiation (W m$^{-2}$), CS is the condensation

158    sink (s$^{-1}$), RH is the relative humidity (%), and k is the reaction rate constant depending on ambient temperature (see detailed

159    definition for k in Eq. (3) of Mikkonen et al., 2011) with coefficients of a = 8.21×10$^{-3}$, b = 0.62, c = 1, and d = -0.13. The

160    $H_2SO_4$ concentration at Zeppelin was 5.98×10$^4$–3.19×10$^6$ molecules cm$^{-3}$ during the summer in 2008 (Giamarelou et al., 2016)

161    which is in a similar range to ours (2.69×10$^4$–7.68×10$^6$ molecules cm$^{-3}$) in 2016-2018.

## 3 Results and discussion

The data coverage for the size distribution data collected by nano-SMPS was about 89% during the 27 months sampling period (Oct 2016 to Dec 2018). The monthly variations of the number concentrations of the 3–20 nm nanoparticles ($N_{3–25}$) and 25–60 nm nanoparticles ($N_{25–60}$) in 2016–2018 (averaged from hourly data) are shown in Figure 2. We compared our nano-SMPS data with DMPS data at the same station as shown in Figure S1 in the Supplement, suggesting that they were in a good agreement. Both $N_{3–25}$ and $N_{25–60}$ were highest in summer and lowest in winter, indicating that NPF occurred frequently in summer. The higher SRAD and lower CS (calculated from the 3–810 nm size distribution data) in summer also favored nanoparticle production. The highest monthly SRAD (199 W m$^{-2}$) was observed in June. Due to the higher latitude of the site, the SRAD was lower than values reported at other continental sites (449 W m$^{-2}$ during NPF in Lanzhou, China (Gao et al, 2011); 442–445 W m$^{-2}$ during NPF in Pallas, Finland (Asmi et al., 2011); and 700 W m$^{-2}$ during NPF in Atlanta, USA (Woo et al., 2001)). The wind speed in summer was lower than in other seasons, as expected from local climatology (Maturilli et al., 2013). In addition, marine biogenic sources, which provide gaseous precursors (e.g., DMS, $H_2SO_4$, and $NH_3$) for nanoparticle formation, were known as abundant in summer. It was observed that the percentage of air mass passing over high chlorophyll-α (MODIS data) region, and $H_2SO_4$ and $NH_3$ concentrations measured at the site increased in summer (Figure S2 and Table S1 in the Supplement). For example, chlorophyll-α concentration (a proxy for marine phytoplankton biomass) in the Arctic Ocean surrounding the observation site from 2016 to 2018 began to increase in April and reached a maximum in May to June (Figure S2 in the Supplement). During the Arctic haze period, the amount of accumulation-mode particles (>100 nm) increased considerably. A significant CS increase occurred in Mar (Figure 2). The high amount of accumulation-mode particles in spring and the high amount of nucleation-mode particles in summer are consistent with previous findings (Tunved et al., 2013; Dall'Osto et al., 2017; Heinzenberg et al., 2017).

The size distributions of the 3–60 nm particles from 2016 to 2018 (hourly data) were classified into several major groups using the k-means clustering method. Four distinct clusters were found (Figure 3 (a)), with mode diameters of around 10 nm (cluster 1), 20 nm (cluster 2), 30 nm (cluster 3), and 50 nm (cluster 4). Cluster 1 included newly formed particles with high population. Cluster 4 had the lowest ultrafine particles concentration, representing the background condition. The frequencies of each cluster by month are shown in Figure 3 (b). The annual average percentages of each cluster were 7% (cluster 1), 15% (cluster 2), 23% (cluster 3), and 55% (cluster 4). The frequencies of clusters 1 and 2 increased significantly and the cluster 2 was often appeared after the cluster 1 in the late spring and summer months (May, June, July, and August), suggesting that strong particle growth (i.e., increases in mode diameter) after NPF occurred during those months.

We identified two distinct types of NPF (Figure 4). In type 1, $N_{3–25}$ increased significantly with subsequent particle growth (the freshly formed particles experienced gradual growth), a typical banana-shaped nucleation event, which is regularly observed at many locations worldwide. In type 2, $N_{3–25}$ increased significantly without clear subsequent particle growth (almost no increase of the mode diameter with time, or not clear for growth); this type of event lasted more than 2 hours. Therefore, the GR could be calculated only for type 1. The cases not matching either of these, they were classified as "undefined" NPF

which $N_{3-25}$ increased for a short period of time (less than 2 hours). This NPF classification approach was similar to methods employed previously (Dal Maso et al., 2005; Kulmala et al., 2012; Nguyen et al., 2016). The mean occurrence percentage of NPF days (all types) per year from 2016 to 2018 was 23%. Dall'Osto et al. (2017) found that the average of yearly NPF occurrence from 2000 to 2010 was 18%, lower than our value, and that this increased over time as the coverage of sea-ice melt increased. Based on Heintzenberg et al. (2017) study, the mean occurrence percentage of NPF days per year from 2006 to 2015 was estimated to be around 20%. In addition, DMS originating from marine sources can be a key precursor contributing to NPF in the remote marine atmosphere (Leaitch et al., 2013; Park et al., 2017; Jang et al., 2019). In the Arctic region, the DMS concentration increased by 33% per decade from 1998 to 2016 (Galí et al., 2019), potentially leading to the increase in the annual NPF occurrence in this area.

It was shown that the concentration of fine particles could be affected by local combustion sources such as local port and cruise ships (Eckhardt et al., 2013). The effects of anthropogenic sources (e.g., downtown, local port, and cruise ship) on the NPF were examined by using local wind and air mass trajectory data to find whether air mass or wind passed over the Ny-Ålesund downtown and local port during NPF events. Also, the concentration of black carbon (BC) at Zeppelin, typically emitted from primary combustion sources, was used to examine the effect of primary combustion sources on the NPF. We found that the air mass and wind passed over the downtown including the local port during only two NPF events out of whole NPF events (170 events). During these two NPF events, the BC concentration little increased. Thus, we believe the effect of anthropogenic sources on the NPF should be small. Also, in our NPF data analysis we filtered out two NPF events having increased BC concentration and wind direction coming from the Ny-Ålesund downtown or port.

The highest percentage of NPF occurrence for all types was observed in August (63%) and June (61%), followed by May (47%) and July (42%) as shown in Figure 5. NPF was observed only occasionally in winter during the Arctic night from November to February, consistent with previous observations (Ström et al., 2009; Heintzenberg et al., 2017). Although NPF occurrence could be expected to be lowest in April due to highest CS (Figure 2), that was not the case. Our results showed that NPF occurrence increased significantly in April, was maintained at a high level from May to August, then decreased in September and October. The average values of CS during NPF event and non-event days were $0.57 \times 10^{-3}$ s$^{-1}$ and $0.69 \times 10^{-3}$ s$^{-1}$, respectively. The higher biological and photochemical activity, lower transport of pollutants from mid-latitudes, and increased wet scavenging of particles (low CS) in summer likely favored NPF (Ström et al., 2009). In addition, the melting of sea ice in summer can increase the availability of marine biogenic sources, promoting NPF (Quinn et al., 2008; Tovar-Sánchez et al., 2010; Dall'Osto et al., 2018). Overall, NPF occurrence is mainly affected by the availability of solar radiation (photochemistry) and gaseous precursors in addition to the survival probability of clusters or particles (Kulmala et al., 2017). In addition, it was suggested that fragmentation of primary marine polymer gels, which are derived from phytoplankton along the marginal ice zone, could be a source for atmospheric nanoparticles (NPF events below 10 nm) in the high Arctic boundary layer (Heintzenberg et al., 2017; Karl et al., 2019; Mashayekhy Rad et al., 2019).

A so-called "weak NPF" event, in which initial formation and growth were completed to < 10 nm without further growth, was observed. The weak NPF events documented here could not be detected in previous studies where the minimum

229 detectable size was ~10 nm. The fraction of weak NPF occurrences (out of all NPF occurrences each month) was highest in

230 April (58%) and October (50%), compared to values in May (20%), June (14%), July (8%), August (15%), and September

231 (25%). In April, this was likely caused by the combination of strong solar radiation (i.e., strong photochemistry for production

232 of condensing vapors responsible for particle growth) and high CS; in contrast, October's combination of the low solar

233 radiation (i.e., weak photochemistry) and low CS led to a similar result.

234 NPF lasted for several hours with similar start times (Figure 5). NPF duration was around 6–7 h on average and was

235 longest in summer. Typically, NPF started between 13:00 and 14:00 (local time), suggesting that photochemical activity with

236 strong solar radiation played an important role in NPF initiation. The variations in start time from month to month (Mar to

237 Nov) were smaller than the monthly variations in NPF occurrence or duration. The nighttime NPF also occurred in late fall to

238 winter (20% out of total NPF events). The exact mechanism for this NPF was unclear. Nanoparticles formed at earlier times

239 (daytime) in other places may be transported to the site during nighttime (Vehkamaki et al., 2004; Park et al., 2020).

240 Figure 6 shows the MODIS monthly chlorophyll-$\alpha$ concentrations around Svalbard, which increased from April and

241 decreased after August, consistent with the NPF occurrence frequency. The chlorophyll-$\alpha$ concentration was intense in the

242 ocean regions southwest and southeast of Svalbard. A recent study revealed that the DMS production capacity of the Greenland

243 Sea (to the southwest) was 3 times greater than that of the Barents Sea (to the southeast) (Park et al., 2018); this is further

244 discussed in the context of air mass trajectory data in a later section. Full monthly values of average chlorophyll-$\alpha$ concentration

245 over the area (70-85ºN, 25ºW-50ºE) and "air mass exposure to chlorophyll-$\alpha$" ($E_{chl}$) which explains the DMS mixing ratio of

246 the air mass arriving at Zeppelin (Park et al., 2018) are summarized in Figure S2 in the Supplement. The $E_{chl}$ provides the

247 measure of potential DMS production capacity of the ocean air mass passed over (Park et al., 2018). It was found that "air

248 mass exposure to chlorophyll-$\alpha$" ($E_{chl}$) was correlated well (r = 0.69 and $p$-value < 0.05; not shown) with the NPF occurrence

249 frequency, compared to the average chlorophyll-$\alpha$ concentration over the area (70-85ºN, 25ºW-50ºE).

250 To determine the characteristics of particle growth, we calculated the GR in the 3–7 nm, 7–25 nm, and 3–25 nm size

251 ranges (i.e., $GR_{3-7}$, $GR_{7-25}$, and $GR_{3-25}$) for NPF events (Figure 7). The average $GR_{3-25}$ for all months was 2.66 nm h$^{-1}$,

252 comparable to previously reported GR data (0.2–4.1 nm h$^{-1}$) in the Arctic region (Kerminen et al., 2018). The highest monthly

253 average $GR_{3-25}$ was observed in July (3.03 nm h$^{-1}$) and the maximum individual value (6.54 nm h$^{-1}$) occurred in June. The

254 averages of $GR_{3-7}$ and $GR_{7-25}$ were 2.07 nm h$^{-1}$ and 2.85 nm h$^{-1}$, respectively. However, the GR was much lower than the values

255 observed in typical urban areas (Table 1), suggesting a lower availability of condensing vapors contributing to particle growth

256 in the Arctic atmosphere. The formation rates of particles in the same size range as calculated GR were also derived. The

257 averages of $J_{3-7}$, $J_{7-25}$, and $J_{3-25}$ during NPF events were 0.04 cm$^{-3}$ s$^{-1}$, 0.09 cm$^{-3}$ s$^{-1}$ and 0.12 cm$^{-3}$ s$^{-1}$, respectively. The highest

258 monthly average and maximum for $J_{3-7}$ were both found in June, but for $J_{7-25}$ and $J_{3-25}$ were found in July. The formation rates

259 (relative standard deviation (RSD) = 39–44%) varied by month more significantly than for GR (RSD = 27–33%). The

260 formation rates in this study were much lower than those reported in continental areas (Stanier et al., 2004; Hamed et al., 2007;

261 Wu et al., 2007; Manninen et al., 2010; Xiao et al., 2015; Shen et al., 2016; Cai et al., 2017). A good linear relationship was

262 found between $J_{3-7}$ and $N_{3-7}$ (r = 0.97 and $p$-value < 0.001) as shown in Figure S3 in the Supplement, indicating that 3–7 nm

8

263  particles were produced by gas-to-particle conversion rather than direct emissions in the particle phase (i.e., not primary)

264  (Kalivitis et al., 2019). No significant correlation was found between $J_{3-7}$ and $GR_{3-7}$, suggesting that the vapors participating

265  in the early stage of NPF could be at least partly different from the vapors contributing to subsequent particle growth (Nieminen

266  et al., 2014). However, detailed chemical data for nanoparticles during formation and growth should be obtained to achieve

267  complete understanding of the participating chemical species. Our data indicate that, although NPF occurrence frequency in

268  the Arctic was comparable to continental areas, the J and GR were much lower. Time series of daily GR and J in different

269  modes ($GR_{3-7}$ and $J_{3-7}$, and $GR_{7-25}$ and $J_{7-25}$), weekly $N_{3-7}$ and $N_{7-25}$, and weekly $NH_3$ and $H_2SO_4$ are shown in Figure S4 in the

270  Supplement.

271       The existence of significant amounts of nanoparticles as small as 3 nm during NPF events at the study site suggests

272  that NPF occurred there, rather than the particles being transported from other regions after growth. In other words, if NPF

273  occurred at other locations far from the study site, the nanoparticles would have grown during transport to the site and few 3

274  nm particles would have been detected there. The lifetime of the 3 nm particles in this study (growth to particles larger than 7

275  nm) was estimated to be 2-3 hours on average. It was reported that nanoparticles (< 5 nm) in the troposphere could survive for

276  several hours or less (Anastasio and Martin, 2001).

277       Five air mass clusters were found (Figure 8 (a)), representing the contributions of different air masses in different

278  seasons: clusters 1, 2, 3, 4, and 5 represented southwest (slow), south (slow), southeast (fast), northwest (fast), and northeast

279  (fast) air masses, respectively. The air mass speed (travel distance/time) was used to determine whether the air mass was slower

280  or faster compared to the average air mass speed during the measurement period. Cluster 1 dominated in summer, when NPF

281  occurrence was highest; it had the lowest air mass speed, the lowest fraction of land influence (15%), and the highest fraction

282  of time spent over the sea (50%) compared to other air mass clusters. Time spent over sea-ice was 35%. The CS values were

283  $0.54 \times 10^{-3}$ s$^{-1}$, $0.74 \times 10^{-3}$ s$^{-1}$, $0.77 \times 10^{-3}$ s$^{-1}$, $0.64 \times 10^{-3}$ s$^{-1}$, and $0.80 \times 10^{-3}$ s$^{-1}$ for cluster 1, cluster 2, cluster 3, cluster 4, and cluster

284  5, respectively., suggesting that cluster 1 had the lowest CS. Our data suggest that a slowly moving air mass, which spent most

285  of the time over the ocean and sea-ice is the most favourable for NPF.

286       We further explored the potential source regions of the air masses in relation to NPF using air mass backward

287  trajectory data and the 75th percentile of $N_{3-25}$ (Figure 8 (b)). Increases in the amount of nanoparticles (i.e., NPF events)

288  occurred more frequently when the air mass passed over the oceanic regions to southwest and south of Svalbard (overall, 49%

289  of the air mass during NPF was southwest, i.e., cluster 1). As shown earlier (Figure 6), the chlorophyll-α concentration was

290  strong in the southwest and southeast ocean regions, and the DMS production capacity of the southwest ocean was 3 times

291  greater than that of the southeast ocean. The DMS production capacity was defined as the potential amount of DMS produced

292  from the phytoplankton biomass (Park et al., 2018). Several previous studies also support the strong DMS production capacity

293  in the southwest ocean (Degerlund and Eilertsen, 2010; Galí and Simó, 2010). These results suggest that marine biogenic

294  sources from the southwest ocean (Greenland Sea) region play an important role in NPF in the Arctic.

295       The DMS in the ocean is produced by complicate microbial food-web processes (Stefels et al., 2007). In general,

296  sea surface DMS maximum occurs following local phytoplankton biomass maxima, thereby leading to lag periods on the order

297 of several weeks to months (so called DMS summer paradox) (Galí and Simó, 2015). This phenomenon could be explained

298 by several key processes: a succession in phytoplankton composition, grazing by zooplankton on DMSP-containing

299 phytoplankton and the bacterial degradation of DMSP into DMS (Polimene et al., 2012). However, a clear temporal correlation

300 between atmospheric (and/or seawater) DMS level and phytoplankton biomass (i.e., chlorophyll-α concentration) has been

301 observed for the ocean domains where the strong DMS-producer (both containing high intra cellular DMSP content and DMSP

302 cleavage enzyme) such as haptophytes and dinoflagellates are predominating (e.g., Arnold et al., 2010; Park et al., 2013; Park

303 et al., 2018; Uhlig et al. 2019; Zhang et al., 2020). Only limited number of phytoplankton class including dinoflagellates and

304 haptophytes possess enzyme that can convert DMSP into DMS during their growth (Alcolombri et al., 2015). In particular,

305 *Emiliania huxleyi* and *Phaeocystis sp.* which are highly abundant haptophyte in high latitude oceans play key roles in

306 controlling global DMS emission because the DMS production capacity of these species is much higher than other globally

307 abundant phytoplankton species (Liss et al., 1994; McParland and Levine, 2019). For example, multi-year measurements of

308 atmospheric DMS mixing ratios at Zeppelin station showed a strong correlation between sea-surface chlorophyll-α

309 concentration (estimated by MODIS-aqua) and atmospheric DMS levels (Park et al., 2013; Park et al., 2018). Furthermore,

310 relationships between the atmospheric DMS and phytoplankton biomass were regionally and temporally varied with the

311 relative abundance of strong DMS(P)-producer (Park et al., 2018). This is because the oceanic DMS production in vicinity of

312 the observation site (i.e., Greenland and Barents Seas) largely governed by direct DMS exudation of phytoplankton that has

313 both high cellular DMSP content and DMSP-cleavage enzyme during phytoplankton bloom period. Recent study conducted

314 at remote Antarctic site also revealed that the number concentration of nano-size particles (3–10 nm in diameter) was positively

315 correlated with the chlorophyll-α concentration during the period when strong DMS-producer predominate (dominance of

316 Phaeocystis > 50%; estimated by PHYSAT algorithm) (Jang et al., 2019).

317 We then examined the chemical characteristics of particulate matter (PM) and daily concentration of gaseous $NH_3$.

318 The seasonal characteristics of ionic species ($Na^+$, $Mg^{2+}$, $K^+$, $NH_4^+$, $NO_3^-$, $SO_4^{2-}$, and $Cl^-$) in PM from 2016 to 2018 (Table S1

319 in the Supplement) revealed that the contributions of primary sea salt particles ($Na^+$, $Mg^{2+}$, and $Cl^-$) increased in winter with

320 high wind speeds, while the contributions of $NH_4^+$, $NO_3^-$, and $SO_4^2$ (secondary species) increased in spring and summer. The

321 slope of the cation equivalents ($Na^+$, $Mg^{2+}$, $K^+$, and $NH_4^+$) versus the anion equivalents ($NO_3^-$, $SO_4^{2-}$, and $Cl^-$) (= 0.98; not

322 shown) suggested that the measured cations were mostly neutralized by the anions (Zhang et al., 2015). These ionic species

323 can exist in large particles, and do not necessarily represent the chemical composition of the nanoparticles, but they can provide

324 information about the overall chemical properties of the particles in different seasons. The non-sea salt sulfate (nss-$SO_4^{2-}$)

325 could have had a secondary origin from the DMS from the sea (Park et al., 2017; Kecorius et al., 2019). The $SO_4^{2-}$ could also

326 come from sea salt particles (primary production of $SO_4^{2-}$) (Karl et al., 2019). Thus, the concentration of nss-$SO_4^{2-}$ was derived

327 from nss-$SO_4^{2-}$ (µg m$^{-3}$) = total $SO_4^{2-}$ (µg m$^{-3}$) – 0.252×$Na^+$ (µg m$^{-3}$) by using the measured $SO_4^{2-}$ and $Na^+$ concentrations (Zhan

328 et al., 2017). The nss-$SO_4^{2-}$ ratio (nss-$SO_4^{2-}$/total $SO_4^{2-}$) was significantly higher on NPF event days than on non-event days

329 (*p*-value < 0.01; Figure 9). The $NH_3$ concentration was higher on NPF event days than on non-event days as shown in Figure

330 9 (*p*-value < 0.001), similar to results shown in Dall'Osto et al. (2017), although daily $NH_3$ concentration was not significantly

correlated with the $N_{3-25}$ as shown in Figure S5 in the Supplement. The $NH_3$ in the Arctic can originate from biological and animal sources (e.g., seabird colonies) (Tovar-Sánchez et al., 2010; Croft et al., 2016; Dall'Osto et al., 2017). The $SO_2$ was not significantly higher on NPF event days than on non-event days (Figure 9), and not significantly correlated with the $N_{3-25}$ (Figure S5 in the Supplement). On the other hand, the $H_2SO_4$ was found to be higher on the NPF event days (Figure 9) and was correlated with the $N_{3-25}$ (Figure S5 in the Supplement), suggesting that the $H_2SO_4$ should play an important role in nucleation and growth. Our data were limited to fully explain the nucleation mechanism. Further studies should be required to elucidate the nucleation mechanism by directly measuring chemical composition of nanoparticles and various precursor vapors.

The NPF event probability distribution with daily CS and temperature was included in Figure S6 in the Supplement. The NPF event probability was calculated by the ratio of the NPF event days per total days for the given CS and temperature. The NPF event probability increased at moderate temperatures when the CS was low, while when the CS was high, the probability increased at relatively high temperature as shown in Figure S6 in the Supplement.

We calculated the NPF criterion ($L_\Gamma$) values for NPF event and non-event days (Figure 10). The seven non-event days when GR could be obtained from pre-existing aerosols were selected for the calculation of the $L_\Gamma$ (Kuang et al., 2010). The NPF duration time was determined using the proposed method (Kulmala et al., 2012), with the time range of non-event days set as daytime (06:00–18:00). When NPF occurred, the $L_\Gamma$ ranged from 0.003–0.27 with a mean and median of 0.044 and 0.041, respectively; all values were less than 1. The $L_\Gamma$ values of non-event days ranged from 0.34–2.59 with a mean and a median of 1.49 and 1.61, respectively; five days were larger than 1. These observations were consistent with previous studies of NPF events in clean or moderately-polluted areas (Tecamac, Atlanta, Boulder, and Hyytiälä), ranging from 0.0075–0.66 (Kuang et al., 2010), and in a highly-polluted area (Beijing), ranging from 0.22–1.75 (Cai et al., 2017). Our data suggest that $L_\Gamma$ can also be useful for determining the occurrence of NPF in the Arctic, but not at 100% certainty. Uncertainties in $H_2SO_4$ concentration inferred from daily $SO_2$ data (as discussed in the experimental section) and other parameters such as the measured GR and averaging time for $L_\Gamma$ (i.e., NPF duration time) could contribute to unclear separation of NPF event and non-event days (Figure 10).


**4 Conclusions**

We examined the characteristics of Arctic NPF at the Mount Zeppelin site by conducting continuous measurements of nanoparticles down to 3 nm size from 2016 to 2018. The size distributions of 3–60 nm particles were classified into distinct clusters with strong seasonal variability and mode diameters of 10 nm (cluster 1), 20 nm (cluster 2), 30 nm (cluster 3), and 50 nm (cluster 4). A significant number of nanoparticles as small as 3 nm often appeared during NPF, particularly in summer, suggesting that there is a good chance that these were produced near the site rather than being transported from other regions after growth. The average NPF occurrence frequency per year was 23%. $J_{3-7}$ averaged 0.04 cm$^{-3}$ s$^{-1}$, ranging from 0.001–0.54 cm$^{-3}$ s$^{-1}$, and $GR_{3-7}$ averaged 2.07 nm h$^{-1}$, ranging from 0.29–5.17 nm h$^{-1}$. These data suggest that the NPF occurrence frequency in the Arctic is comparable to those in continental areas although the J and GR were lower in the Arctic. We next identified

363 five major air mass clusters using backward trajectory analysis; PSCF results indicated that air masses from the south and
364 southwest ocean regions were related to the elevated concentrations of nanoparticles at the site. This region was consistent
365 with elevated chlorophyll-$\alpha$ and DMS production capacity, suggesting that marine biogenic sources should play an important
366 role in Arctic NPF. The concentrations of $NH_3$ and $H_2SO_4$ were higher on NPF event days than on non-event days. Previously
367 developed NPF criteria (a low ratio of loss rate to growth rate of clusters favors NPF) were applicable to Arctic NPF occurrence.
368

379

380 *Data availability.* The nano-SMPS data (3–60 nm) are available in Korea Polar Data Center (KPDC) web site
381 ('https://kpdc.kopri.re.kr/search/'), and the raw data can be distributed upon request to the corresponding author
382 (kpark@gist.ac.kr). The DMPS (5–810 nm and 10–790 nm) data are available in Stockholm University and Norwegian
383 Institute for Air Research (NILU). The meteorological data for solar radiation (SRAD) were provided by the Alfred Wegener
384 Institute (Maturilli, 2019).
385

386 *Competing interests.* The authors declare that they have no conflict of interest.
387

388 **References**

389 Aas, W., M. Fiebig, S., Solberg and K. E. Yttri.: Monitoring of long-range transported air pollutants in Norway. Annual report
390     2018, NILU rapport, 2019.
391 Alcolombri, U., Ben-Dor, S., Feldmesser, E., Levin, Y., Tawfik, D. S., and Vardi, A.: Identification of the algal dimethyl
392     sulfide-releasing enzyme: a missing link in the marine sulfur cycle, Science, 348, 1466–1469,
393     https://doi.org/10.1126/science.aab1586, 2015.

Anastasio, C. and Martin, S. T.: Atmospheric Nanoparticles, Rev. Mineral. Geochem., 44 (1), 293-349, http://doi.org/10.2138/rmg.2001.44.08, 2001.

Arnold, S. R., Spracklen, D. V., Gebhardt, S., Custer, T., Williams, J., Peeken, I., and Alvain, S.: Relationships between atmospheric organic compounds and air-mass exposure to marine biology, Environ. Chem., 7(3), 232-241, https://dx.doi.org/10.1071/EN09144, 2010

Asmi, E., Kivekäs, N., Kerminen, V. M., Komppula, M., Hyvärinen, A. P., Hatakka, J., Viisanen, Y., and Lihavainen, H.: Secondary new particle formation in Northern Finland Pallas site between the years 2000 and 2010, Atmos. Chem. Phys., 11 (24), 12959-12972, https://doi.org/10.5194/acp-11-12959-2011, 2011

Asmi, E., Kondratyev, V., Brus, D., Laurila, T., Lihavainen, H., Backman, J., Vakkari, V., Aurela, M., Hatakka, J., Viisanen, Y., Uttal, T., Ivakhov, V., and Makshtas, A.: Aerosol size distribution seasonal characteristics measured in Tiksi, Russian Arctic, Atmos. Chem. Phys., 16 (3), 1271-1287, https://doi.org/10.5194/acp-16-1271-2016, 2016.

Beddows, D. C., Dall'Osto, M., and Harrison, R. M.: Cluster analysis of rural, urban, and curbside atmospheric particle size data, Environ. Sci. Technol., 43 (13), 4694-4700, https://doi.org/10.1021/es803121t, 2009.

Beine, H., Argentini, S., Maurizi, A., Mastrantonio, G., and Viola, A.: The local wind field at Ny-Ålesund and the Zeppelin mountain at Svalbard, Meteorol. Atmos. Phys., 78 (1-2), 107-113, https://doi.org/10.1007/s007030170009, 2001.

Cai, R., Yang, D., Fu, Y., Wang, X., Li, X., Ma, Y., Hao, J., Zheng, J., and Jiang, J.: Aerosol surface area concentration: A governing factor in new particle formation in Beijing, Atmos. Chem. Phys., 17 (20), 12327-12340, https://doi.org/10.5194/acp-17-12327-2017, 2017.

Covert, D. S., Wiedensohler, A., Aalto, P., Heintzenberg, J., Mcmurry, P. H., and Leck, C.: Aerosol number size distributions from 3 to 500 nm diameter in the arctic marine boundary layer during summer and autumn, Tellus Ser. B-Chem. Phys. Meteorol., 48 (2), 197-212, https://doi.org/10.3402/tellusb.v48i2.15886, 1996.

Croft, B., Martin, R. V., Leaitch, W. R., Tunved, P., Breider, T. J., D'Andrea, S. D., and Pierce, J. R.: Processes controlling the annual cycle of Arctic aerosol number and size distributions, Atmos. Chem. Phys., 16 (6), 3665-3682, https://doi.org/10.5194/acp-16-3665-2016, 2016.

Dal Maso, M., Kulmala, M., Riipinen, I., Wagner, R., Hussein, T., Aalto, P. P., and Lehtinen, K. E.: Formation and growth of fresh atmospheric aerosols: eight years of aerosol size distribution data from SMEAR II, Hyytiälä, Finland, Boreal Environ. Res., 10 (5), 323-336, 2005.

Dall'Osto, M., Beddows, D. C. S., Tunved, P., Krejci, R., Strom, J., Hansson, H. C., Yoon, Y. J., Park, K. T., Becagli, S., Udisti, R., Onasch, T., CD, O. D., Simo, R., and Harrison, R. M.: Arctic sea ice melt leads to atmospheric new particle formation, Sci. Rep., 7 (1), 3318, https://doi.org/10.1038/s41598-017-03328-1, 2017.

Dall'Osto, M., Geels, C., Beddows, D. C. S., Boertmann, D., Lange, R., Nojgaard, J. K., Harrison, R. M., Simo, R., Skov, H., and Massling, A.: Regions of open water and melting sea ice drive new particle formation in North East Greenland, Sci. Rep., 8 (1), 6109, https://doi.org/10.1038/s41598-018-24426-8, 2018.

427 Degerlund, H. and Eilertsen, H. C.: Main Species Characteristics of Phytoplankton Spring Blooms in NE Atlantic and Arctic

428     Waters (68-80ºN), Estuaries Coasts, 33, 242-269, http://dx.doi.org/10.1007/s12237-009-9167-7, 2010.

429 Eckhardt, S., Hermansen, O., Grythe, H., Fiebig, M., Stebel, K., Cassiani, M., Baecklund, A., and Stohl, A.: The influence of

430     cruise ship emissions on air pollution in Svalbard a harbinger of a more polluted Arctic? Atmos. Chem. Phys., 13, 8401-

431     8409, https://doi.org/10.5194/acp-13-8401-2013, 2013.

432 EMEP/CCC: Manual for sampling and chemical analysis, Norwegian Institute for Air Research, Kjeller, EMEP/CCC Report

433     1/95 (Last rev. 2001), http://tarantula.nilu.no/projects/ccc/, 2001.

434 Fleming, Z. L., Monks, P. S., and Manning, A. J.: Untangling the influence of air-mass history in interpreting observed

435     atmospheric composition, Atmos. Res., 104, 1-39, https://doi.org/10.1016/j.atmosres.2011.09.009, 2012.

436 Gao, J., Chai, F., Wang, T., and Wang, W.: Particle number size distribution and new particle formation (NPF) in Lanzhou,

437     Western China, Particuology, 9 (6), 611-618, https://doi.org/10.1016/j.partic.2011.06.008, 2011.

438 Galí, M. and Simó R.: Occurrence and cycling of dimethylated sulfur compounds in the Arctic during summer receding of the

439     ice edge, Mar. Chem., 122 (1-4), 105-117, https://doi.org/10.1016/j.marchem.2010.07.003, 2010.

440 Galí, M. and Simó R.: A metaanalysis of oceanic DMS and DMSP cycling processes: Disentangling the summer paradox,

441     Global Biogeochem. Cycles, 29, 496–515, https://doi.org/10.1002/2014GB004940, 2015.

442 Galí, M., Devred, E., Babin, M., and Levasseur, M.: Decadal increase in Arctic dimethylsulfide emission, Proc. Natl. Acad.

443     Sci. U. S. A., 116 (39), 19311-19317, https://doi.org/10.1073/pnas.1904378116, 2019.

444 Giamarelou, M., Eleftheriadis, K., Nyeki, S., Tunved, P., Torseth, K., and Biskos, G.: Indirect evidence of the composition of

445     nucleation mode atmospheric particles in the high Arctic, J. Geophys. Res. Atmos., 121, 965-975,

446     https://doi.org/10.1002/2015JD023646, 2016.

447 Gong, Y., Hu, M., Cheng, Y., Su, H., Yue, D., Liu, F., Wiedensohler, A., Wang, Z., Kalesse, H., Liu, S., Wu, Z., Xiao, Z., Mi,

448     P., and Zhang, Y.: Competition of coagulation sink and source rate: New particle formation in the Pearl River Delta of

449     China, Atmos. Environ., 44, 3278-3285, https://doi.org/10.1016/j.atmosenv.2010.05.049, 2010.

450 Hamed, A., Joutsensaari, J., Mikkonen, S., Sogacheva, L., Maso, M. D., Kulmala, M., Cavalli, F., Fuzzi, S., Facchini, M., and

451     Decesari, S.: Nucleation and growth of new particles in Po Valley, Italy, Atmos. Chem. Phys., 7 (2), 355-376,

452     https://doi.org/10.5194/acp-7-355-2007, 2007.

453 Heintzenberg, J., Leck, C., and Tunved, P.: Potential source regions and processes of the aerosol in the summer Arctic, Atmos.

454     Chem. Phys., 15 (6), 6487-6502, https://doi.org/10.5194/acp-15-6487-2015, 2015.

455 Heintzenberg, J., Tunved, P., Galí, M., and Leck, C.: New particle formation in the Svalbard region 2006–2015, Atmos. Chem.

456     Phys., 17 (10), 6153-6175, https://doi.org/10.5194/acp-17-6153-2017, 2017.

457 Hirdman, D., Burkhart, J. F., Sodemann, H., Eckhardt, S., Jefferson, A., Quinn, P. K., Sharma, S., Ström, J., and Stohl, A.:

458     Long-term trends of black carbon and sulphate aerosol in the Arctic: changes in atmospheric transport and source region

459     emissions, Atmos. Chem. Phys., 10 (19), 9351-9368, https://doi.org/10.5194/acp-10-9351-2010, 2010.

Hussein, T., Dal Maso, M., Petaja, T., Koponen, I. K., Paatero, P., Aalto, P. P., Hameri, K., and Kulmala, M.: Evaluation of an automatic algorithm for fitting the particle number size distributions, Boreal Environ. Res., 10 (5), 337-355, 2005.

Iziomon, M., Lohmann, U., and Quinn, P.: Summertime pollution events in the Arctic and potential implications, J. Geophys. Res. Atmos., 111, D12206, https://doi.org/10.1029/2005JD006223, 2006.

Jang, E., Park, K.-T., Yoon, Y. J., Kim, T.-W., Hong, S.-B., Becagli, S., Traversi, R., Kim, J., and Gim, Y.: New particle formation events observed at the King Sejong Station, Antarctic Peninsula – Part 2: Link with the oceanic biological activities, Atmos. Chem. Phys., 19, 7595-7608, https://doi.org/10.5194/acp-19-7595-2019, 2019

Järvinen, E., Virkkula, A., Nieminen, T., Aalto, P. P., Asmi, E., Lanconelli, C., Busetto, M., Lupi, A., Schioppo, R., Vitale, V., Mazzola, M., Petäjä, T., Kerminen, V. M., and Kulmala, M.: Seasonal cycle and modal structure of particle number size distribution at Dome C, Antarctica, Atmos. Chem. Phys., 13 (15), 7473-7487, https://doi.org/10.5194/acp-13-7473-2013, 2013.

Jeffries, M. and Richter-Menge, J.: State of the climate in 2011: The Arctic., Bull. Am. Meteorol. Soc., 93, S127-S148, https://doi.org/10.1175/2012BAMSStateoftheClimate.1, 2012.

Kalivitis, N., Kerminen, V.-M., Kouvarakis, G., Stavroulas, I., Tzitzikalaki, E., Kalkavouras, P., Daskalakis, N., Myriokefalitakis, S., Bougiatioti, A., Manninen, H. E., Roldin, P., Petäjä, T., Boy, M., Kulmala, M., Kanakidou, M., and Mihalopoulos, N.: Formation and growth of atmospheric nanoparticles in the eastern Mediterranean: Results from long-term measurements and process simulations, Atmos. Chem. Phys., 19 (4), 2671-2686, https://doi.org/10.5194/acp-19-2671-2019, 2019.

Karl, M., Leck, C., Coz, E., and Heintzenberg, J.: Marine nanogels as a source atmospheric nanoparticles in the high Arctic, Geophys. Res. Lett., 40, 3738-374., https://doi.org/10.1002/grl.50661, 2013.

Karl, M., Leck, C., Mashayekhy Rad, F., Bäcklund, A., Lopez-Aparicio, S., and Heintzenberg, J.: New insights in sources of the sub-micrometre aerosol at Mt. Zeppelin observatory (Spitsbergen) in the year 2015, Tellus Ser. B-Chem. Phys. Meteorol., 71:1, 1613143, https://doi.org/10.1080/16000889.2019.1613143, 2019.

Kecorius S., Vogl, T., Paasonen, P., Lampilahti, J., Rothenberg, D., Wex. H., Zeppenfeld, S., van Pinxteren, M., Hartmann, M., Henning, S., Gong, X., Welti, A., Kulmala, M., Stratmann, F., Herrmann, H., and Wiedensohler, A.: New particle formation and its effect on cloud condensation nulei abundance in the summer Arctic: a case study in the Fram Strait and Barents Sea, Atmos. Chem. Phys., 19, 14339-14364, https://doi.org/10.5194/acp-19-14339-2019, 2019.

Kerminen, V.-M., Chen, X., Vakkari, V., Petäjä, T., Kulmala, M., and Bianchi, F.: Atmospheric new particle formation and growth: review of field observations, Environ. Res. Lett., 13 (10), https://doi.org/10.1088/1748-9326/aadf3c, 2018.

Kuang, C., Riipinen, I., Sihto, S. L., Kulmala, M., McCormick, A. V., and McMurry, P. H.: An improved criterion for new particle formation in diverse atmospheric environments, Atmos. Chem. Phys., 10 (17), 8469-8480, https://doi.org/10.5194/acp-10-8469-2010, 2010.

492 Kuang, C., Chen, M., Zhao, J., Smith, J., McMurry, P. H., and Wang, J.: Size and time-resolved growth rate measurements of
493     1 to 5 nm freshly formed atmospheric nuclei, Atmos. Chem. Phys., 12 (7), 3573-3589, https://doi.org/10.5194/acp-12-
494     3573-2012, 2012.

495 Kulmala, M., Vehkamäki, H., Petäjä, T., Dal Maso, M., Lauri, A., Kerminen, V. M., Birmili, W., and McMurry, P. H.:
496     Formation and growth rates of ultrafine atmospheric particles: a review of observations, J. Aerosol Sci., 35 (2), 143-176,
497     https://doi.org/10.1016/j.jaerosci.2003.10.003, 2004.

498 Kulmala, M., Petaja, T., Nieminen, T., Sipila, M., Manninen, H. E., Lehtipalo, K., Dal Maso, M., Aalto, P. P., Junninen, H.,
499     Paasonen, P., Riipinen, I., Lehtinen, K. E., Laaksonen, A., and Kerminen, V. M.: Measurement of the nucleation of
500     atmospheric aerosol particles, Nature Protocols, 7 (9), 1651-1667, https://doi.org/10.1038/nprot.2012.091, 2012.

501 Kulmala, M., Kerminen, V. M., Petaja, T., Ding, A. J., and Wang, L.: Atmospheric gas-to-particle conversion: why NPF events
502     are observed in megacities?, Faraday Discuss, 200, 271-288, https://doi.org/10.1039/C6FD00257A, 2017.

503 Law, K. S. and Stohl, A.: Arctic air pollution: Origins and impacts, Science, 315 (5818), 1537-1540, https://doi.org/
504     10.1126/science.1137695, 2007.

505 Leaitch, W. R., Sharma, S., Huang, L., Toom-Sauntry, D., Chivulescu, A., Macdonald, A. M., von Salzen, K., Pierce, J. R.,
506     Bertram, A. K., and Schroder, J. C.: Dimethyl sulfide control of the clean summertime Arctic aerosol and cloud, Elem.
507     Sci. Anth., 1, http://doi.org/10.12952/journal.elementa.000017, 2013.

508 Liss, P.S., Malin, G., Turner, S.M., and Holligan, P.M., Dimethyl sulphide and Phaeocystis: a review, J. Mar. Syst., 5 (1), 41–
509     53, https://doi.org/10.1016/0924-7963(94)90015-9, 1994.

510 Manninen, H. E., Nieminen, T., Asmi, E., Gagné, S., Häkkinen, S., Lehtipalo, K., Aalto, P., Vana, M., Mirme, A., Mirme, S.,
511     Hõrrak, U., Plass-Dülmer, C., Stange, G., Kiss, G., Hoffer, A., Törő, N., Moerman, M., Henzing, B., de Leeuw, G.,
512     Brinkenberg, M., Kouvarakis, G. N., Bougiatioti, A., Mihalopoulos, N., amp, apos, Dowd, C., Ceburnis, D., Arneth, A.,
513     Svenningsson, B., Swietlicki, E., Tarozzi, L., Decesari, S., Facchini, M. C., Birmili, W., Sonntag, A., Wiedensohler, A.,
514     Boulon, J., Sellegri, K., Laj, P., Gysel, M., Bukowiecki, N., Weingartner, E., Wehrle, G., Laaksonen, A., Hamed, A.,
515     Joutsensaari, J., Petäjä, T., Kerminen, V. M., and Kulmala, M.: EUCAARI ion spectrometer measurements at 12 European
516     sites – analysis of new particle formation events, Atmos. Chem. Phys., 10 (16), 7907-7927, https://doi.org/10.5194/acp-
517     10-7907-2010, 2010.

518 Maturilli, M., Herber, A., and König-Langlo, G.: Climatology and time series of surface meteorology in Ny-Ålesund, Svalbard,
519     Earth System Science Data, 5, 155-163, https://doi.org/10.5194/essd-5-155-2013, 2013.

520 Maturilli, M.: Basic and other measurements of radiation and continuous meteorological observations at station Ny-Ålesund
521     (2016-2018), reference list of 72 datasets. Alfred Wegener Institute - Research Unit Potsdam, PANGAEA,
522     doi.pangaea.de/10.1594/PANGAEA.908444, 2019.

523 Mashayekhy Rad, F., Zurita, J., Gilles, P., Rutgeerts, L. A. J., Nilsson, U., Ilag, L. L., and Leck, C.: Measurements of
524     Atmospheric Proteinaceous Aerosol in the Arctic Using a Seletive UHPLC/ESI-MS/MS Strategy, J. Am. Soc. Mass
525     Spectrom., 30(1), 161-173, https://doi.org/10.1007/s13361-019-02137-2, 2019.

McParland, E. L.and Levine, N. M.: The role of differential DMSP production and community composition in predicting variability of global surface DMSP concentrations. Limnol. Oceanogr., 64, 757–773, https://doi.org/10.1002/lno.11076, 2019.

McMurry, P. H., Fink, M., Sakurai, H., Stolzenburg, M. R., Mauldin, R. L., Smith, J., Eisele, F., Moore, K., Sjostedt, S., Tanner, D., Huey, L. G., Nowak, J. B., Edgerton, E., and Voisin, D.: A criterion for new particle formation in the sulfur-rich Atlanta atmosphere, J. Geophys. Res, 110, https://doi.org/10.1029/2005JD005901, 2005.

Merikanto, J., Spracklen, D., Mann, G., Pickering, S., and Carslaw, K.: Impact of nucleation on global CCN, Atmos. Chem. Phys., 9 (21), 8601-8616, https://doi.org/10.5194/acp-9-8601-2009, 2009.

Mikkonen, S., Romakkaniemi, S., Smith, J. N., Korhonen, H., Petäjä, T., Plass-Duelmer, C., Boy, M., McMurry, P. H., Lehtinen, K. E. J., Joutsensaari, J., Hamed, A., Mauldin Iii, R. L., Birmili, W., Spindler, G., Arnold, F., Kulmala, M., and Laaksonen, A.: A statistical proxy for sulphuric acid concentration, Atmos. Chem. Phys., 11 (7), 20141-20179, https://doi.org/10.5194/acp-11-11319-2011, 2011.

Neuber, R., Ström, J., Hübner, C., Hermansen, O., Arya, B. C., Beichen, Z., Kallenborn, R., Karasinki, G., Ivanov, B., and Moen, J.: Atmospheric research in Ny-Ålesund-a flagship programme, Norsk Polarinstitutt, 2011.

Nguyen, Q. T., Glasius, M., Sørensen, L. L., Jensen, B., Skov, H., Birmili, W., Wiedensohler, A., Kristensson, A., Nøjgaard, J. K., and Massling, A.: Seasonal variation of atmospheric particle number concentrations, new particle formation and atmospheric oxidation capacity at the high Arctic site Villum Research Station, Station Nord, Atmos. Chem. Phys., 16 (17), 11319-11336, https://doi.org/10.5194/acp-16-11319-2016, 2016.

Nieminen, T., Asmi, A., Dal Maso, M., Aalto, P. P., Keronen, P., Petäjä, T., Kulmala, M., and Kerminen, V.-M.: Trends in atmospheric new-particle formation: 16 years of observations, Boreal Environ. Res., 19, 191-214, 2014.

O'Neill, N., Pancrati, O., Baibakov, K., Eloranta, E., Batchelor, R., Freemantle, J., McArthur, L., Strong, K., and Lindenmaier, R.: Occurrence of weak, sub-micron, tropospheric aerosol events at high Arctic latitudes, Geophys. Res. Lett., 35 (14), L14814, https://doi.org/10.1029/2008GL033733, 2008.

Park, K.-T., Lee, K., Yoon, Y.-J., Lee, H.-W., Kim, H.-C., and Lee, B.-Y., Hermansen, O., Kim, T.-W, Holmén, K.: Linking atmospheric dimethyl sulphide and the Arctic Ocean spring bloom, Geophys. Res. Lett., 40, 155-160, https://doi.org/10.1029/2012GL054560, 2013.

Park, K.-T., Jang, S., Lee, K., Yoon, Y. J., Kim, M.-S., Park, K., Cho, H.-J., Kang, J.-H., Udisti, R., and Lee, B.-Y.: Observational evidence for the formation of DMS-derived aerosols during Arctic phytoplankton blooms, Atmos. Chem. Phys., 17 (15), 9665-9675, https://doi.org/10.5194/acp-17-9665-2017, 2017.

Park, K. T., Lee, K., Kim, T. W., Yoon, Y. J., Jang, E. H., Jang, S., and Lee, B. Y., Hermansen, O.: Atmospheric DMS in the Arctic Ocean and its relation to phytoplankton biomass, Glob. Biogeochem. Cycles, 32 (3), 351-359, https://doi.org/10.1002/2017GB005805, 2018.

Park, J., Dall'Osto, M., Park, K., Gim, Y., Kang, H. J., Jang, E., Park, K.-T., Park, M., Yum, S. S., Jung, J., Lee, B. Y., and Yoon, Y. J.: Shipborne observations reveal contrasting Arctic marine, Arctic terrestrial and Pacific marine aerosol properties, Atmos. Chem. Phys., 20, 5573-5590, https://doi.org/10.5194/acp-20-5573-2020, 2020.

Pekney, N. J., Davidson, C. I., Zhou, L., and Hopke, P. K.: Application of PSCF and CPF to PMF-modeled sources of $PM_{2.5}$ in Pittsburgh, Aerosol Sci. Technol., 40 (10), 952-961, https://doi.org/10.1080/02786820500543324, 2007.

Polimene, L., Archer, S. D., Butenschön, M., Allen, J. I.: A mechanistic explanation of the Sargasso Sea DMS "summer paradox", Biogeochemistry, 110, 243–255, https://doi.org/10.1007/s10533-011-9674-z, 2012.

Quinn, P., Miller, T., Bates, T., Ogren, J., Andrews, E., and Shaw, G.: A 3-year record of simultaneously measured aerosol chemical and optical properties at Barrow, Alaska, J. Geophys. Res: Atmospheres, 107 (D11), 4130, https://doi.org/10.1029/2001JD001248, 2002.

Quinn, P., Shaw, G., Andrews, E., Dutton, E., Ruoho-Airola, T., and Gong, S.: Arctic haze: current trends and knowledge gaps, Tellus Ser. B-Chem. Phys. Meteorol., 59 (1), 99-114, https://doi.org/10.1111/j.1600-0889.2006.00238.x, 2007.

Quinn, P., Bates, T., Baum, E., Bond, T., Doubleday, N., Fiore, A. M., Flanner, M., Fridlind, A., Garrett, T. J., Koch, D., Menon, S., Shindell, D., Stohl, A., and Warren, S. G.: Short-Lived Pollutants in the Arctic: their climate impact and possible mitigation strategies, Atmos. Chem. Phys., 8, 1723-1735, https://doi.org/10.5194/acp-8-1723-2008, 2008.

Radke, L. F., Lyons, J. H., Hegg, D. A., Hobbs, P. V., and Bailey, I. H.: Airborne observations of Arctic aerosols. I: Characteristics of Arctic haze, Geophys. Res. Lett., 11 (5), 393-396, https://doi.org/10.1029/GL011i005p00393, 1984.

Satheesh, S., Moorthy, K. K.: Radiative effects of natural aerosols: A review, Atmos. Environ., 39 (11), 2089-2110, https://doi.org/10.1016/j.atmosenv.2004.12.029, 2005.

Sharma, S., Ishizawa, M., Chan, D., Lavoué, D., Andrews, E., Eleftheriadis, K., and Maksyutov, S.: 16-year simulation of Arctic black carbon: Transport, source contribution, and sensitivity analysis on deposition, J. Geophys. Res. Atmos., 118 (2), 943-964, https://doi.org/10.1029/2012JD017774, 2013.

Shaw, G. E.: The Arctic haze phenomenon, Bull. Amer. Meteorol. Soc., 76 (12), 2403-2414, https://doi.org/10.1175/1520-0477(1995)076<2403:TAHP>2.0.CO,2, 1995.

Shen, L., Wang, H., Lu, S., Li, L., Yuan, J., Zhang, X., Tian, X., and Tang, Q.: Observation of aerosol size distribution and new particle formation at a coastal city in the Yangtze River Delta, China, Sci. Total Environ., 565, 1175-1184, https://doi.org/10.1016/j.scitotenv.2016.05.164, 2016.

Shen, X., Sun, J., Zhang, X., Zhang, Y., Zhang, L., and Fan, R.: Key features of new particle formation events at background sites in China and their influence on cloud condensation nuclei, Front. Environ. Sci Eng., 10 (5), https://doi.org/10.1007/s11783-016-0833-2, 2016.

Stanier, C. O., Khlystov, A. Y., and Pandis, S. N.: Nucleation Events During the Pittsburgh Air Quality Study: Description and Relation to Key Meteorological, Gas Phase, and Aerosol Parameters, Aerosol Sci. Technol., 38 (sup1), 253-264, https://doi.org/10.1080/02786820390229570, 2004.

591    Stefels, J., Steinke, M., Turner, S., Malin, G., and Belviso, S.: Environmental constraints on the production and removal of the

592        climatically active gas dimethylsulphide (DMS) and implications for ecosystem modelling, Biogeochemistry, 83 (1),

593        245–275, https://doi.org/10.1007/s10533-007-9091-5, 2007.

594    Ström, J., Umegård, J., Tørseth, K., Tunved, P., Hansson, H. C., Holmén, K., Wismann, V., Herber, A., and König-Langlo,

595        G.: One year of particle size distribution and aerosol chemical composition measurements at the Zeppelin Station,

596        Svalbard, March 2000–March 2001, Phys. Chem. Earth, Parts A/B/C 2003, 28 (28-32), 1181-1190,

597        https://doi.org/10.1016/j.pce.2003.08.058, 2003.

598    Ström, J., Engvall, A.-C., Delbart, F., Krejci, R., and Treffeisen, R.: On small particles in the Arctic summer boundary layer:

599        observations at two different heights near Ny-Ålesund, Svalbard, Tellus Ser. B-Chem. Phys. Meteorol., 61 (2), 473-482,

600        https://doi.org/10.3402/tellusb.v61i2.16845, 2009.

601    IPCC, 2014: Climate Change 2014: Synthesis Report. Contribution of Working Groups I, II and III to the Fifth Assessment

602        Report of the Intergovernmental Panel on Climate Change [Core Writing Team, R.K. Pachauri and L.A. Meyer (eds.)].

603        IPCC, Geneva, Switzerland, 151 pp.

604    Toon, O. B. and Pollack, J. B.: Atmospheric aerosols and climate: Small particles in the Earth's atmosphere interact with visible

605        and infrared light, altering the radiation balance and the climate, American Scientist, 68 (3), 268-278,

606        https://www.jstor.org/stable/27849822, 1980.

607    Tovar-Sánchez, A., Duarte, C. M., Alonso, J. C., Lacorte, S., Tauler, R., and Galbán-Malagón, C.: Impacts of metals and

608        nutrients released from melting multiyear Arctic sea ice, J. Geophys. Res., 115 (C7),

609        https://doi.org/10.1029/2009JC005685, 2010.

610    Tunved, P., Ström, J., and Krejci, R.: Arctic aerosol life cycle: linking aerosol size distributions observed between 2000 and

611        2010 with air mass transport and precipitation at Zeppelin station, Ny-Ålesund, Svalbard, Atmos. Chem. Phys., 13 (7),

612        3643-3660, https://doi.org/10.5194/acp-13-3643-2013, 2013.

613    Uhlig, C., Damm, E., Peeken, I., Krumpen, T., Rabe, B., Korhenon, M., and Ludwichowski, K.-U.: Sea Ice and Water Mass

614        Influence Dimethylsulfide Concentration in the Central Arctic Ocean, Front. Earth Sci., 7, 179,

615        https://doi.org/10.3389/feart.2019.00179, 2019.

616    Vehkamäki, H., Dal Maso, M., Hussein, T., Flanagan, R., Hyvärinen, A., Lauros, J., Merikanto, P., Mönkkönen, M., Pihlatie,

617        K., Salminen, K., Sogacheva, L., Thum, T., Ruuskanen, T. M., Keronen, P., Aalto, P. P., Hari, P., Lehtinen, K. E. J.,

618        Rannik, Ü., and Kulmala, M.: Atmospheric particle formation events at Värriö measurement station in Finnish Lapland

619        1998–2002, Atmos. Chem. Phys., 4, 2015–2023, https://doi.org/10.5194/acp-4-2015-2004, 2004.

620    Venzac, H., Sellegri, K., Laj, P., Villani, P., Bonasoni, P., Marinoni, A., Cristofanelli, P., Calzolari, F., Fuzzi, S., and Decesari,

621        S.: High frequency new particle formation in the Himalayas, Proc. Natl. Acad. Sci., 105 (41), 15666-15671,

622        https://doi.org/10.1073/pnas.0801355105, 2008.

623 Wang, Y., Zhang, X., and Draxler, R. R.: TrajStat: GIS-based software that uses various trajectory statistical analysis methods
624       to identify potential sources from long-term air pollution measurement data, Environ. Modelling Softw., 24 (8), 938-939,
625       https://doi.org/10.1016/j.envsoft.2009.01.004, 2009.

626 Wang, Z., Wu, Z., Yue, D., Shang, D., Guo, S., Sun, J., Ding, A., Wang, L., Jiang, J., Guo, H., Gao, J., Cheung, H. C.,
627       Morawska, L., Keywood, M., and Hu, M.: New particle formation in China: Current knowledge and further directions,
628       Sci. Total Environ., 577, 258-266, https://doi.org/10.1016/j.scitotenv.2016.10.177, 2017.

629 Weller, R., Schmidt, K., Teinilä, K., and Hillamo, R.: Natural new particle formation at the coastal Antarctic site Neumayer,
630       Atmos. Chem. Phys., 15 (19), 11399-11410, https://doi.org/10.5194/acp-15-11399-2015, 2015.

631 Wiedensohler, A., Covert, D. S., Swietlicki, E., Aalto, P., Heintzenberg, J., and Leck, C.: Occurrence of an ultrafine particle
632       mode less than 20 nm in diameter in the marine boundary layer during Arctic summer and autumn, Tellus Ser. B-Chem.
633       Phys. Meteorol., 48 (2), 213-222, https://doi.org/10.3402/tellusb.v48i2.15887, 1996.

634 Willis, M. D., Burkart, J., Thomas, J. L., Köllner, F., Schneider, J., Bozem, H., Hoor, P. M., Aliabadi, A. A., Schulz, H., and
635       Herber, A. B.: Growth of nucleation mode particles in the summertime Arctic: a case study, Atmos. Chem. Phys., 16 (12),
636       7663-7679, https://doi.org/10.5194/acp-16-7663-2016, 2016.

637 Woo, K. S., Chen, D. R., Pui, D. Y. H., and McMurry, P. H.: Measurement of Atlanta Aerosol Size Distributions: Observations
638       of Ultrafine Particle Events, Aerosol Sci. Technol., 34 (1), 75-87, https://doi.org/10.1080/02786820120056, 2010.

639 Wu, Z., Hu, M., Liu, S., Wehner, B., Bauer, S., Ma ßling, A., Wiedensohler, A., Petäjä, T., Dal Maso, M., and Kulmala, M.:
640       New particle formation in Beijing, China: Statistical analysis of a 1-year data set, J. Geophys. Res.: Atmos., 112 (D9),
641       https://doi.org/10.1029/2006JD007406, 2007.

642 Xiao, S., Wang, M. Y., Yao, L., Kulmala, M., Zhou, B., Yang, X., Chen, J. M., Wang, D. F., Fu, Q. Y., Worsnop, D. R., and
643       Wang, L.: Strong atmospheric new particle formation in winter in urban Shanghai, China, Atmos. Chem. Phys., 15 (4),
644       1769-1781, https://doi.org/10.5194/acp-15-1769-2015, 2015.

645 Yu, H., Ren, L., and Kanawade, V. P.: New particle formation and growth mechanisms in highly polluted environments, Curr.
646       Pollut. Rep., 3 (4), 245-253, https://doi.org/10.1007/s40726-017-0067-3, 2017.

647 Zhan, J., Li, W., Chen, L., Lin, Q., and Gao, Y.: Anthropogenic influences on aerosols at Ny-Ålesund in the summer Arctic,
648       Atmos. Pollut. Res., 8, 383-393, http://dx.doi.org/10.1016/j.apr.2016.10.010, 2017.

649 Zhang, Y., Zhang H.-H., Yang G.-P., and Liu Q-L.: Chemical Characteristics and Source Analysis of Aerosol Composition
650       over the Bohai Sea and the Yellow Sea in Spring and Autumn, J. Atmos. Sci., 72 (9), 3563-3573,
651       https://doi.org/10.1175/JAS-D-14-0372.1, 2015.

652 Zhang, M., Park, K.-T., Lin, Q., Yan, J., Park, K., Wu, Y., Chen, L., Jang, E., Gao, W., Tan, G., and Wang, J: Atmospheric
653       dimethyl sulfide and its significant influence on the sea-to-air flux calculation over the Southern Ocean. Prog. Oceanogr.,
654       186, https://doi.org/10.1016/j.pocean.2020.102392, 2020.
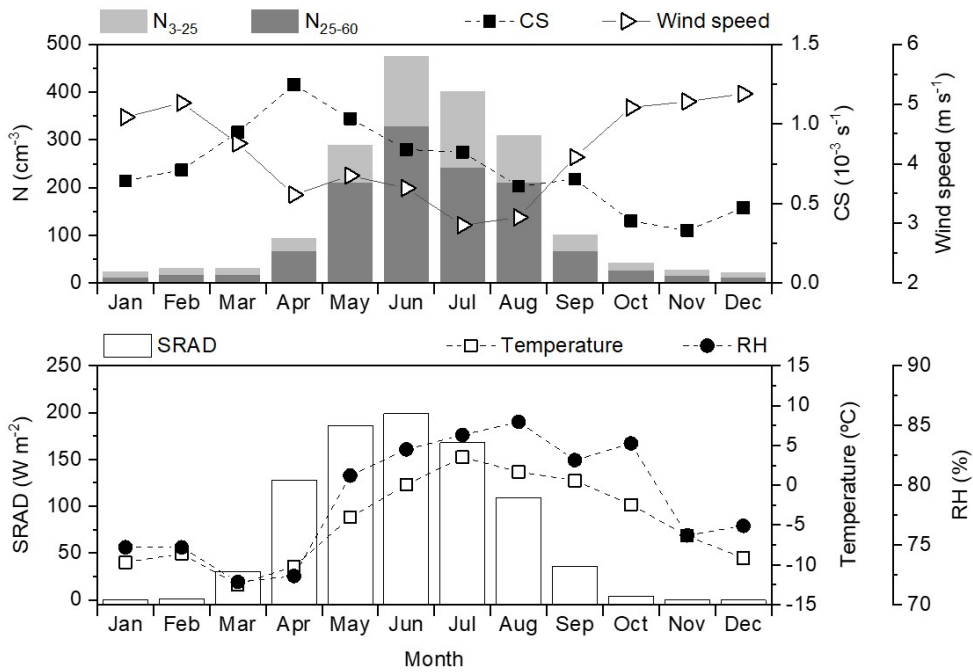
655
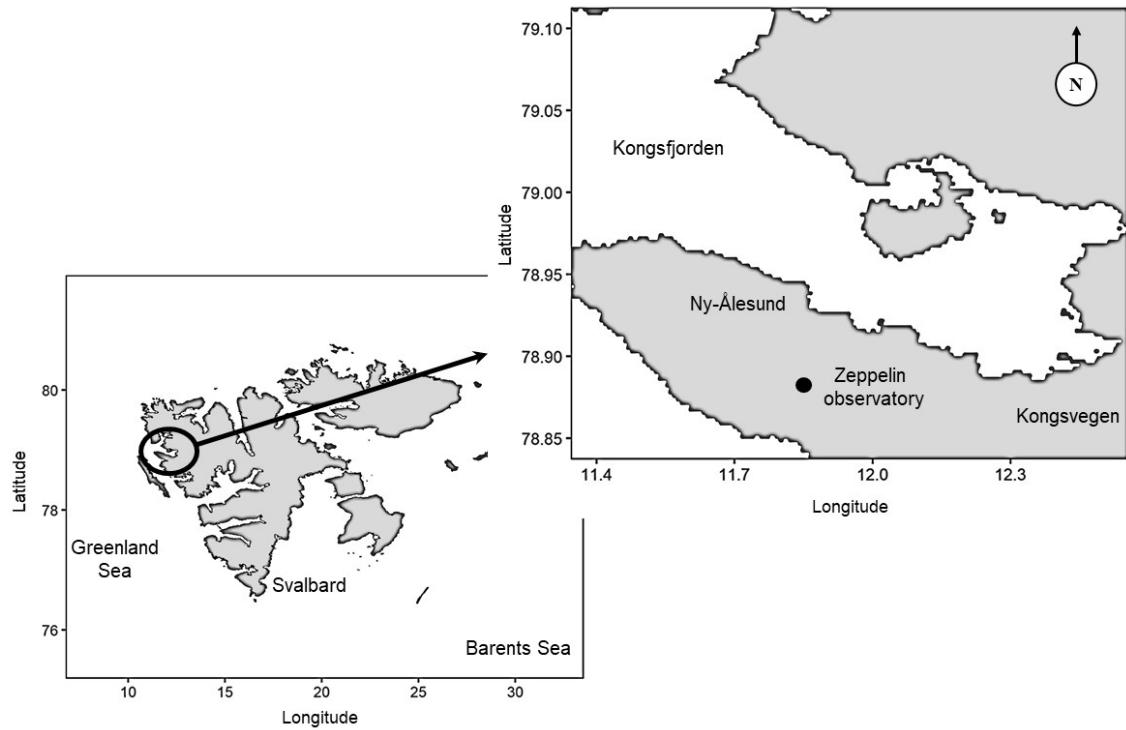
656

657   Figure 1. Measurement site (Zeppelin Observatory) in the Svalbard Archipelago, Ny-Ålesund, Norway.
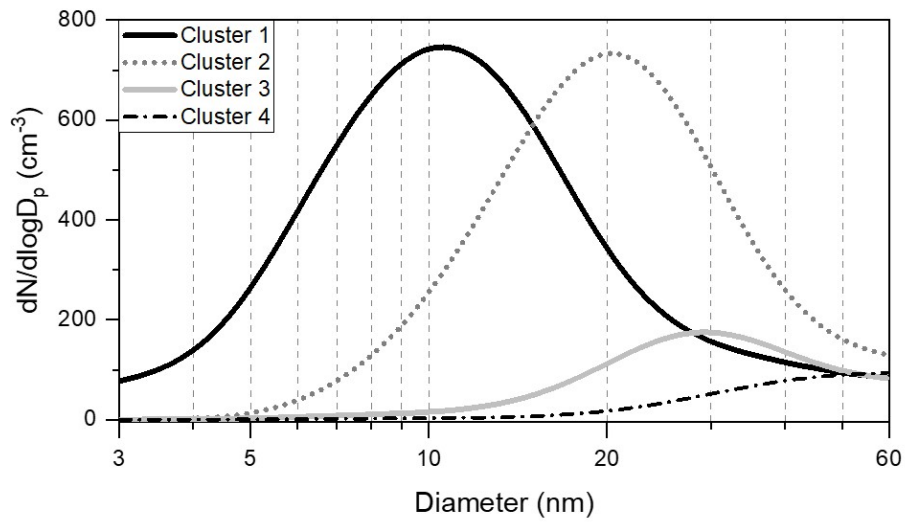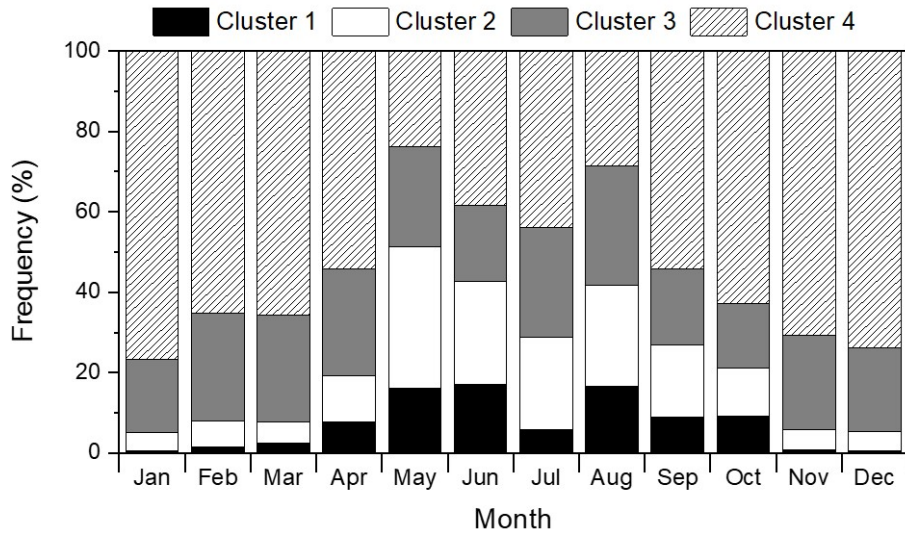
658

659

660    Figure 2. Monthly variations of $N_{3–25}$, $N_{25–60}$, CS, and wind speed (upper panel), temperature, RH, and SRAD (lower panel)
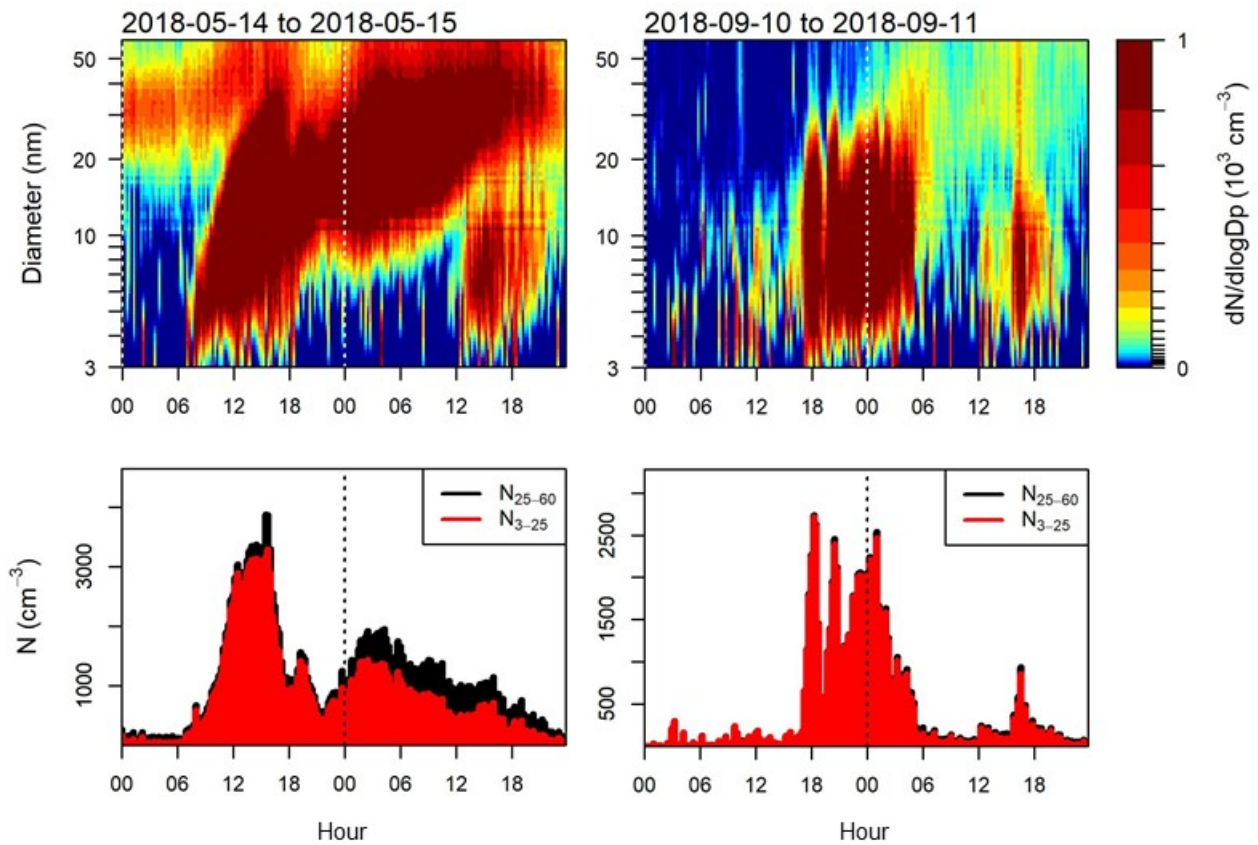
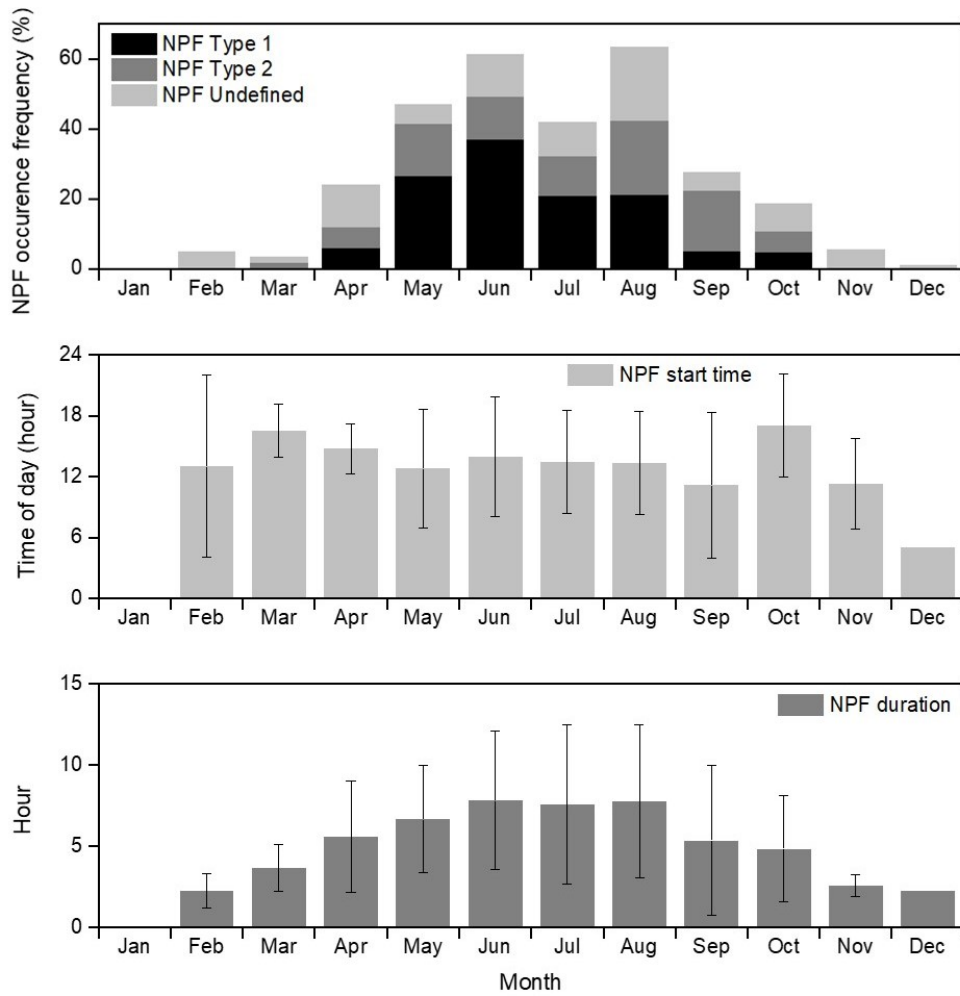661    from 2016 to 2018.

662

663
664

(a)



665
666

(b)

667    Figure 3. Major particle clusters by (a) size distribution and (b) monthly frequency of clusters from 2016 to 2018.
668

669

Figure 4. Examples of distinct NPF types identified in this study. In type 1 (left), $N_{3-25}$ increases significantly with continuous particle growth, while in type 2 (right) it increases significantly without significant particle growth. The x-axis is the local time (hour).
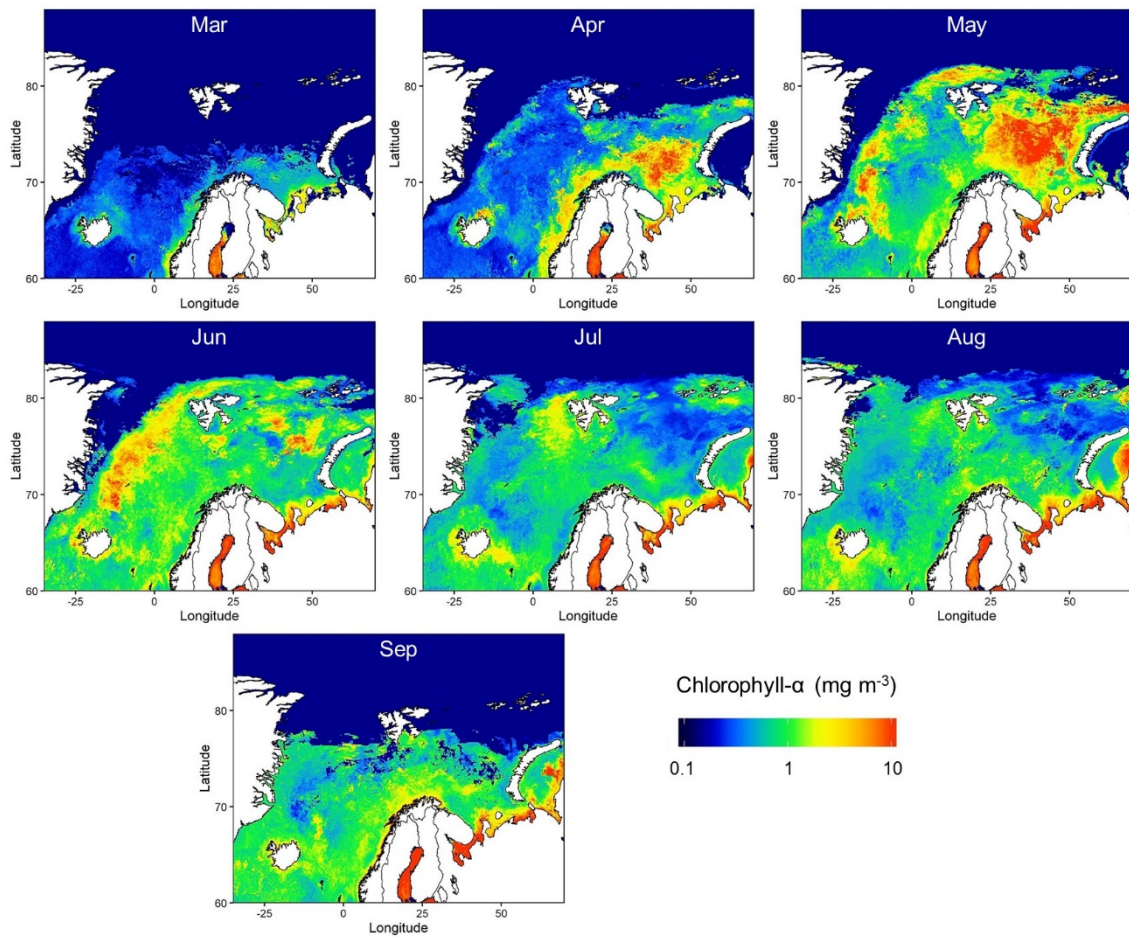
673

24

674

675 Figure 5. Monthly variations of NPF occurrence, start time (local time), and duration; the error bar represents standard
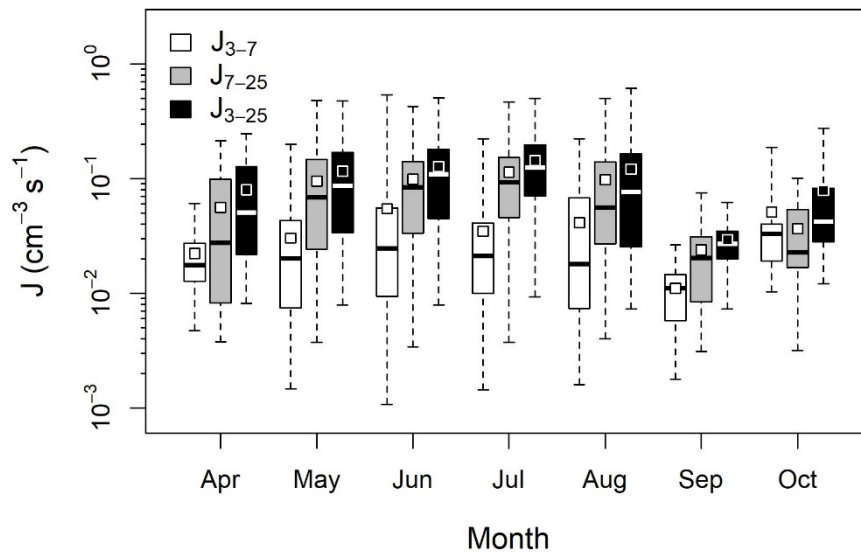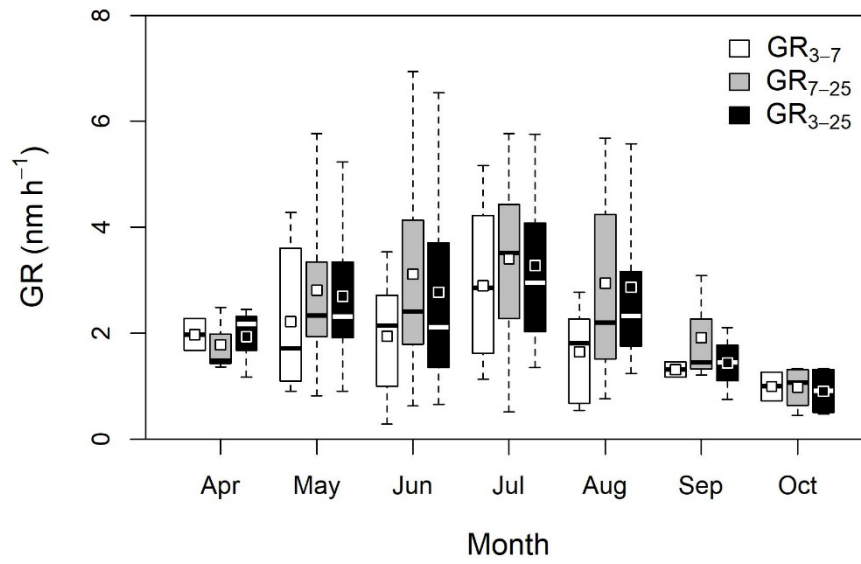
676 deviation.

677

678

679　Figure 6. MODIS-derived monthly chlorophyll-α concentration from 2016 to 2018 at 4 km resolution.
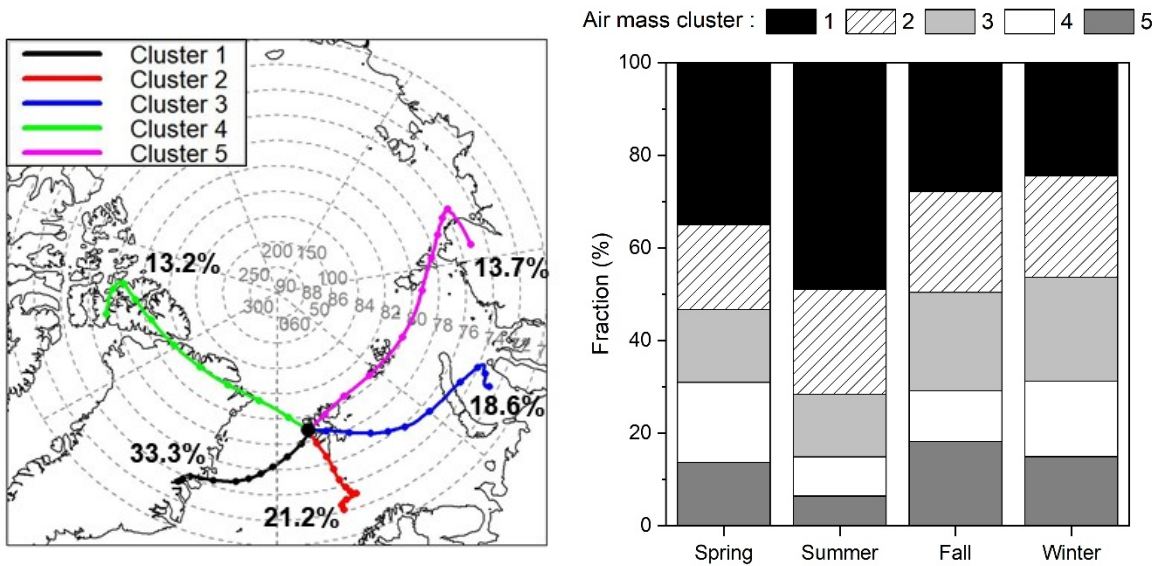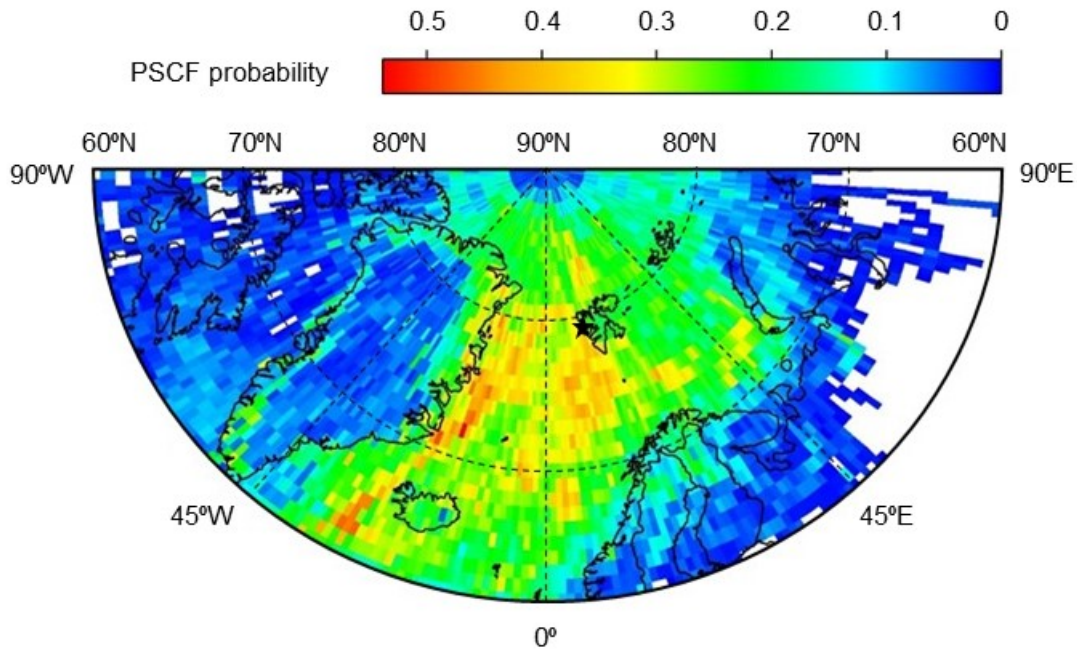
680

681

682

683



684

685  Figure 7. Monthly variations of GR$_{3-7}$, GR$_{7-25}$, GR$_{3-25}$, J$_{3-7}$, J$_{7-25}$, and J$_{3-25}$ for NPF in the Arctic. Boxes and whiskers represent

686  the 25$^{th}$–75$^{th}$ percentiles and minimum–maximum, respectively; squares indicate means and horizontal lines within boxes
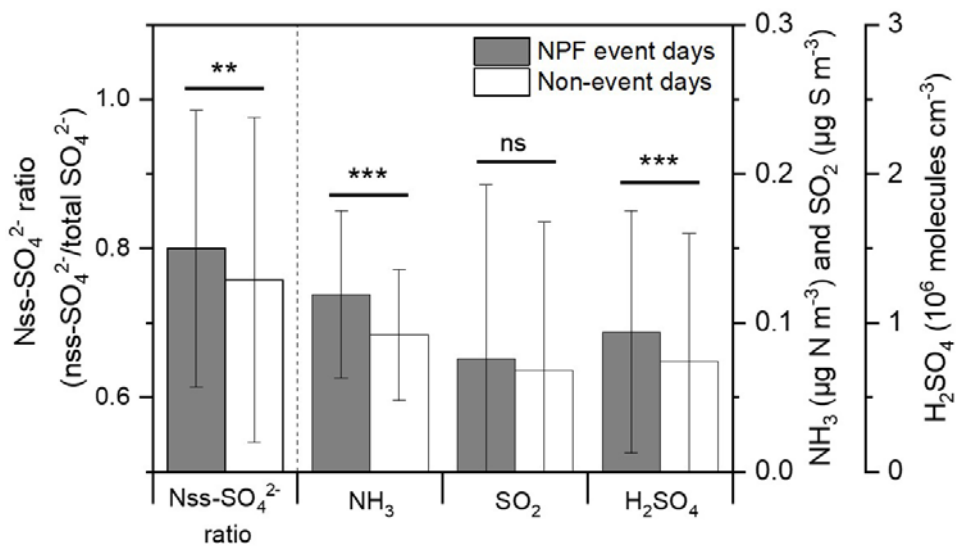
687  indicate medians.

688

689
690 (a)



691
692 (b)

693  Figure 8. (a) Five major clusters for air mass back trajectories from 2016 to 2018 and the fraction of each cluster by seasons.

694  (b) PSCF back-trajectory analysis for air mass origins affecting NPF at the 75th percentile of $N_{3-25}$.

695

28

Figure 9. Comparison of average nss-$SO_4^{2-}$ ratio (nss-$SO_4^{2-}$/total $SO_4^{2-}$), $NH_3$, $SO_2$, and $H_2SO_4$ concentrations between NPF events and non-event days: error bar and stars represent the standard deviation and $p$-values of a t-test (ns: $> 0.05$, *: $\leq 0.05$, **: $\leq 0.01$, ***: $\leq 0.001$), respectively.
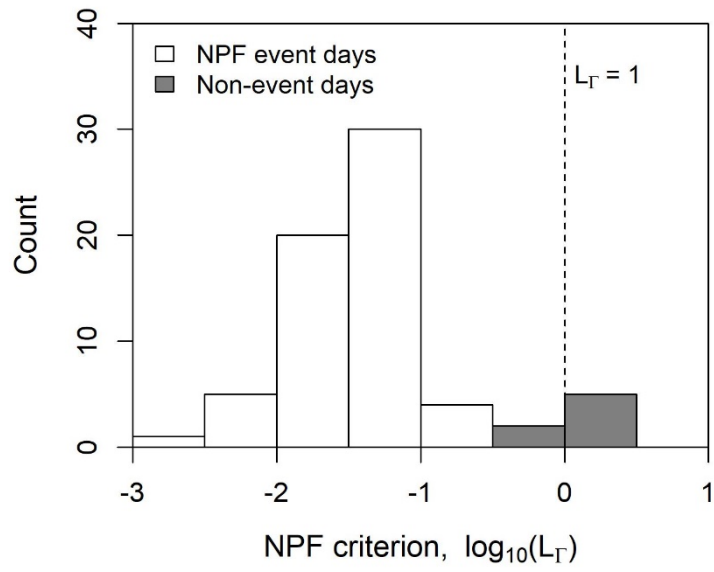
701

702    Figure 10. Distribution of NPF criterion ($L_\Gamma$) values for NPF event days (white) and non-event days (grey) in the Arctic.

703

Table 1. Summary of NPF frequency, J, and GR at various sampling sites, including the present study.

| Site name and characteristics | | Period | NPF frequency | GR (nm h$^{-1}$) | | J (cm$^{-3}$ s$^{-1}$) | | Reference |
|---|---|---|---|---|---|---|---|---|
| Zeppelin, Norway | Arctic | 2016 to 2018 | 23% | GR$_{3-7}$ GR$_{7-25}$ GR$_{3-25}$ | 0.29–5.17 0.45–6.94 0.48–6.54 | J$_{3-7}$ J$_{7-25}$ J$_{3-25}$ | 0.001–0.54 0.003–0.50 0.007–0.61 | This study |
| Finokalia, Greece | Marine background | Jun 2008 to Jun 2018 | 27% | GR$_{9-25}$ | 5.4±3.9 | J$_{9-25}$ | 0.9±1.2 | Kalivitis et al. (2019) |
| Beijing, China | Urban | Mar 2004 to Feb 2005 | 40% | GR$_{3-25}$ | 0.1–11.2 | J$_{3-25}$ | 3.3–81.4 | Wu et al. (2007) |
| Pittsburgh, USA | Urban | Jul 2001 to Jun 2002 | 30% | N/A | N/A | N/A | N/A | Stanier et al. (2004) |
| San Pietro Capofiume, Italy | Sub-urban | Mar 2002 to Mar 2005 | 36% | GR$_{3-20}$ | 2.9–22.9 | J$_{3-20}$ | 0.2–36.9 | Hamed et al. (2007) |
| 12 European sites (EUCAARI project)[a] | Rural and background | 2008 to 2009 | 21–57% | GR$_{7-20}$ | 3.6–6.8 | J$_{2-3}$ | 0.7–32.4 | Manninen et al. (2010) |
| Hyytiälä, Finland | Rural | 1996 to 2003 | >24% | GR$_{3-25}$ | 0.9–5.3 | J$_{3-25}$ | 0.2–1.1 | Dal Maso et al. (2005) |
| ShangDianzi station, China | Rural | Mar 2008 to Dec 2013 | 36% | GR$_{3-25}$ | 0.7–13.4 | J$_{3-25}$ | 0.5–39.3 | Shen et al. (2016) |
| Pyramid, Nepal | Himalayas | Mar 2006 to Aug 2007 | >35% | GR$_{10-20}$ | 1.8 ± 0.7 | J$_{10-20}$ | 0.05–0.2 | Venzac et al. (2008) |
| Dome C | Antarctica | Dec 2007 to Nov 2009 | 5–54% | GR$_{10-25}$ | 0.5–4.6 | J$_{10-25}$ | 0.022–0.11 | Järvinen et al. (2013) |

| | | | | | | | | |
|---|---|---|---|---|---|---|---|---|
| Neumayer | Antarctica | Jan 2012 to Mar 2012 Feb 2014 to Apr 2014 | N/A | $GR_{3-25}$ | 0.4–1.9 | $J_{3-25}$ | 0.02–0.1 | Weller et al. (2015) |
| King Sejong | Antarctica | Mar 2009 to Dec 2016 | 6% | $GR_{10-25}$ | 0.02–3.09 | $J_{2.5-10}$ | 0.16-9.88 | Kim et al. (2019) |
| Nord, Greenland | Arctic | Jul 2010 to Feb 2013 | 17–38% | N/A | N/A | N/A | N/A | Nguyen et al. (2016) |

705 [a] Pallas and Hyytiälä (Finland), Vavihill (Sweden), Mace Head (Ireland), Cavauw (Netherlands), Melpitz and Hohenpeissenberg (Germany), K-Puszta (Hungary), Jungfraujoch (Switzerland), Puy de Dome (France), San Pietro Capofiume (Italy), and Finokalia (Greece).